OVERFLOW
Turbulence Model Resource
Verification Results

Marissa L. Childs
Thomas H. Pulliam
Dennis C. Jespersen

NASA/Ames Research Center
Mail Stop 258-2
Bldg. 258, Rm. 146
P.O. Box 1
Moffett Field, CA 94035-0001

June 18, 2014

Abstract

We exercise the computational fluid dynamics code OVERFLOW on four test cases from the NASA/Langley Turbulence Model Resource web site: 2D zero pressure gradient flat plate, 2D planar shear, 2D bump-in-channel, and 3D bump-in-channel. The goal is turbulence model verification for OVERFLOW.

1   Introduction

The purpose of this study is to perform turbulence model verification for OVERFLOW using the NASA Langley Research Center Turbulence Modeling Resource (TMR) test cases [1]. Some of the discussion and text given below is taken directly from the TMR website, (all due credit to Dr. Chris Rumsey,

1

NASA/LaRC, and his colleagues). The approach described here uses the TMR-provided cases and grids. For OVERFLOW we made every attempt to apply the same flow conditions and boundary conditions as prescribed at the TMR website, to enable comparison with results from CFL3D [2] and FUN3D [3]. We assess the OVERFLOW implementation of the Spalart-Allmaras (SA) and Menter Shear Stress Transport (SST) turbulence models, with specific versions and modifications detailed below. We used version 2.2g of OVERFLOW. The CFL3D and FUN3D results given here are taken directly from the TMR website.

From the TMR website: "The purpose here is to provide a large sequence of nested grids of the same family, along with results from existing CFD codes that employ specific forms of particular turbulence models, in order to help programmers verify their implementations of these same models. On a given grid, there may be differences between the results from different codes, but presumably as the grid is refined the results should approach the same answer (if the flow conditions and boundary conditions are the same). With **verification**, the purpose is not to establish the "goodness" of a model compared to experiment, but rather to establish that a model has been implemented correctly, as intended according to the equations and boundary conditions. (It is through **validation** that a model's "goodness" is established.) Because the purpose here is primarily verification, experiment is not specifically looked at, although law-of-the-wall theory is included for the sake of reference."

To the best of our knowledge, there has been no previous systematic attempt at turbulence model verification for OVERFLOW. This work aims to check that the correct turbulence models have been used in OVERFLOW and that they are coded correctly. If results from OVERFLOW agree with results from CFL3D and FUN3D then we gain increased confidence that the turbulence models in OVERFLOW are implemented correctly.

For each of the test cases in this report, a very fine structured grid was given, from which coarser grids were created by deleting every other grid line. All codes used the same grids. CFL3D is a cell-centered code which uses structured grids, while FUN3D is a node-centered code which can use quadrilateral and hexahedral elements.

Note that much of the text and some of the figures presented below are taken directly from the TMR website and, in some cases, were updated to reflect the addition of the OVERFLOW results.

2   2D Zero Pressure Gradient Flat Plate

In this section we present turbulence model verification for Overflow performed using the LaRC Turbulence Modeling Resource (TMR) 2D flat plate test case. This case has $M = 0.2$, and Reynolds number $Re = 5$ million based on a grid length of 1. The body reference length is 2 units. Because the solid wall of the grid extends from $x = 0$ to $x = 2$, this means that Re_x at $x = 1$ is 5 million, and Re_x at $x = 2$ (the downstream end of the plate) is 10 million. Figure 1 shows the layout of the simple flat plate grids used for this study, along with the boundary conditions. (Note that particular variations of the boundary conditions (BCs) at the inflow, top wall, and outflow may also work and yield similar results for this problem.)
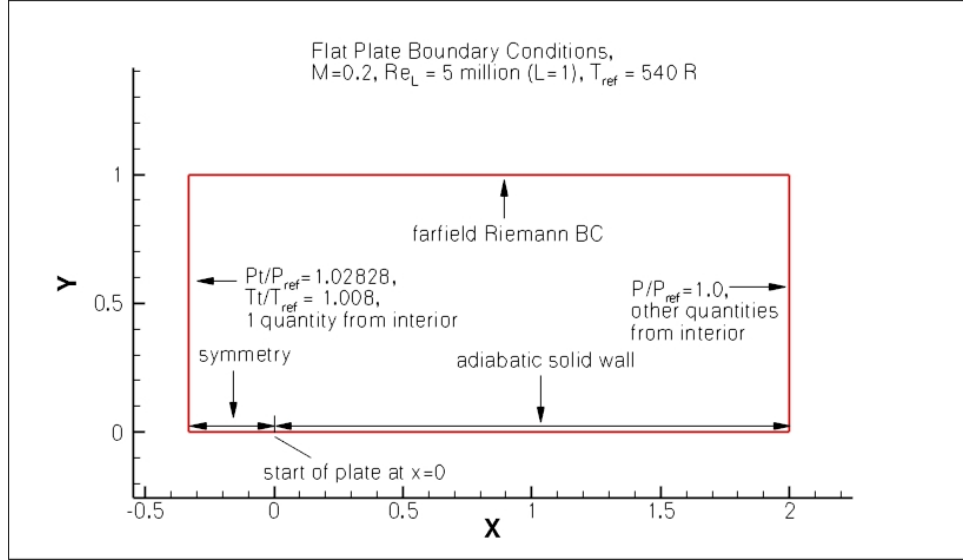
Figure 1: Flat plate geometry and boundary conditions.

The grids are taken directly from the TMR website; details on the formats and other characteristics are available there. Two-dimensional structured grids usable by Overflow [4] are given with dimensions as follows:

- 545×385 (449 points on solid plate; this grid is sometimes referred to as L0)

- 273×193 (225 points on solid plate, denoted L1)

- 137×97 (113 points on solid plate, denoted L2)

- 69×49 (57 points on solid plate, denoted L3)

- 35×25 (29 points on solid plate, denoted L4)

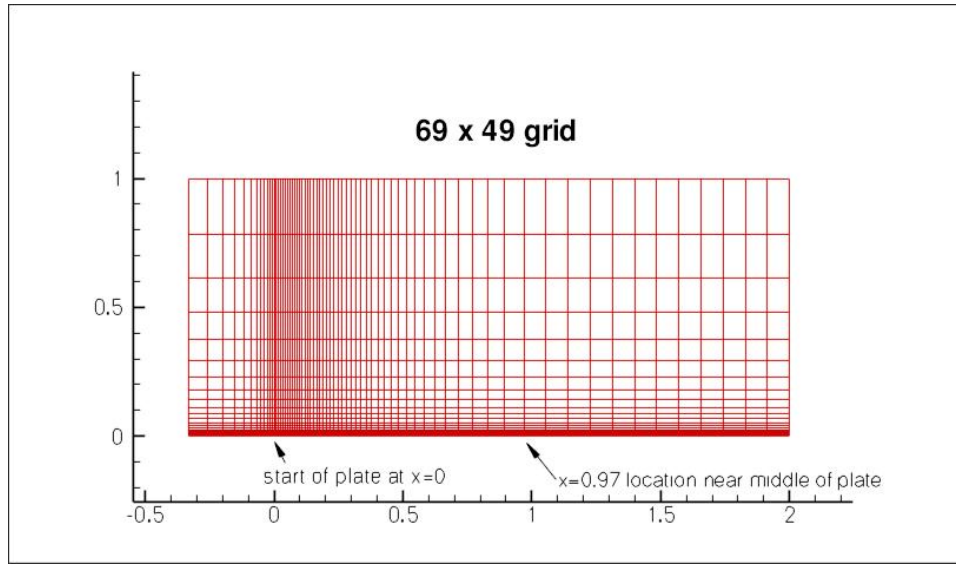For example, the 69×49 grid is shown in Figure 2.

Figure 2: Grid system for flat plate.

The TMR website provides expected CFL3D and FUN3D results for the SA [5] and SST-V [6] models as defined in the TMR turbulence model specifications, SA [7] and SST-V [8].

The grids provided were put into the three-plane two-dimensional format used by OVERFLOW , and input files were generated for the cases with the appropriate boundary and flow conditions. Matrix dissipation with low-Mach preconditioning was used. A sample OVERFLOW input file for the finest grid SST-V case is shown here:

```
&GLOBAL
    NSTEPS= 12000,  RESTRT= .F.,
    MULTIG= .T.,  FMG   = .T.,  FMGCYC= 50,50,  NGLVL = 2,
    NQT   = 205,
```

4

```
      /
&FLOINP
     FSMACH= 0.2,  REY   = 5.E6,  XKINF = 2.25E-7, MUTINF = 0.01,
      /
&VARGAM /

&GRDNAM
     NAME  = 'TMR Flat Plate SST-V',
      /
&NITERS /
&METPRM
     IDISS = 4,  BIMIN = -1,
      /
&TIMACU
     DT    = 1.0,  CFLMIN= 25,
      /
&SMOACU
     DIS2  = 0,  DIS4  = 0.01,
      /
&VISINP
     CFLT  = 4, FSOT = 1, ISTRAIN = 1,
      /
&BCINP
     IBTYP =  1,  5, 47, 41, 33, 21,
     IBDIR =  2,  2, -2,  1, -1,  3,
     JBCS  =  1, 97,  1,  1, -1,  1,
     JBCE  = 96, -1, -1,  1, -1, -1,
     KBCS  =  1,  1, -1,  1,  1,  1,
     KBCE  =  1,  1, -1, -1, -1, -1,
     LBCS  =  2,  2,  2,  2,  2,  1,
     LBCE  = -2, -2, -2, -2, -2,  1,
     BCPAR1(4) = 1.0, BCPAR2(4) = 1.0, BCPAR1(5) = 1.0,
      /
&SCEINP /
```

We used a modification of OVERFLOW version 2.2g, where a value of 1 for the new variable ISTRAIN selects the SST-V model. This is standard starting with version 2.2h of OVERFLOW.

2.1 Overflow Flat Plate SA Results

Typical convergence histories are shown in Figure 3, where we strove to reach machine zero whenever possible. As discussed on the TMR website, "The codes were not run to machine-zero iterative convergence, but an attempt was made to converge sufficiently so that results of interest were well within normal engineering tolerance and plotting accuracy. For example, for CFL3D the density residual was typically driven down below 10^{-13}."

(a) Flow Solver Residual Convergence   (b) Turbulence Model Convergence
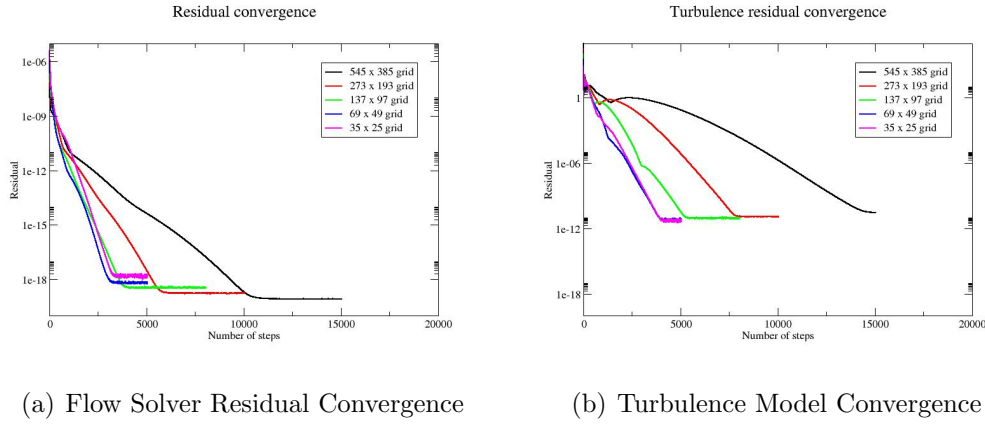
Figure 3: SA convergence characteristics, flat plate.

In the CFL3D and FUN3D tests reported below, the turbulent inflow boundary condition used for SA was $\widehat{\nu}_{farfield} = 3\nu_\infty$. For OVERFLOW the freestream eddy viscosity was set to 0.2, which is consistent with the CFL3D and FUN3D results.

Figure 4 shows the drag coefficient for CFL3D FUN3D and OVERFLOW on the four finer-resolution grids. For each code, the drag coefficient converges as the grid is refined, and the codes are consistent with one another.

Figure 5 shows the convergence of the surface skin friction coefficient C_f at $x = 0.97008$ as a function of grid size for the three codes. The x-coordinate is $1/N^{\frac{1}{2}}$, which is proportional to grid spacing h. At the left of the plot, $h = 0$ represents an infinitely fine grid. As can be seen, both CFL3D and OVERFLOW approach from above and FUN3D approaches from below, but all three go toward approximately the same result as the mesh is refined.

Figure 6 shows the convergence of the drag coefficient at $x = 0.97008$ as

6
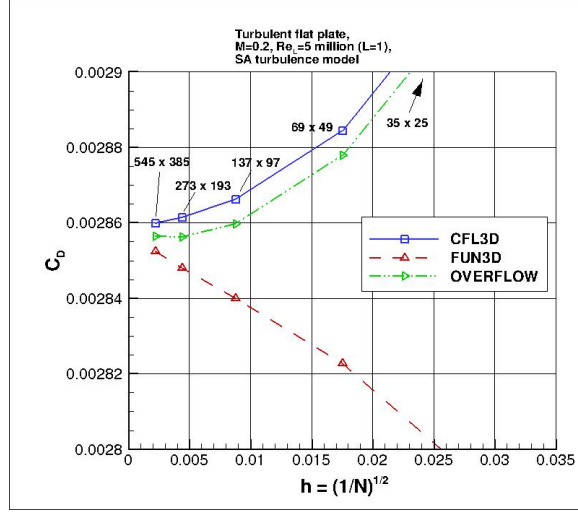
Figure 4: SA drag convergence, flat plate.
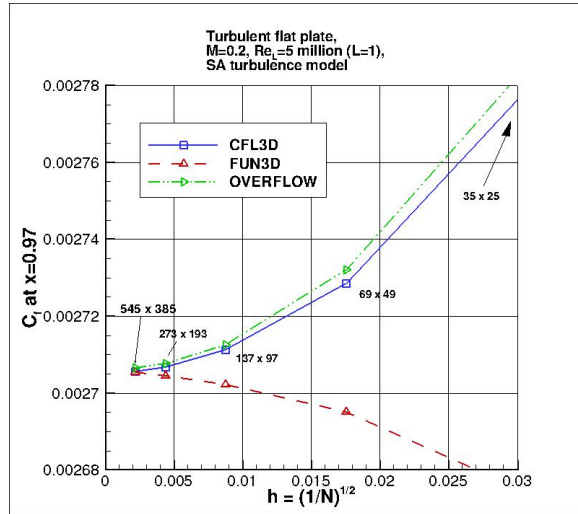
Figure 5: SA grid convergence, C_f at $x = 0.97$.

a function of grid size for the three codes. The drag coefficient is convergent as the grid is refined, and the codes are consistent with one another.
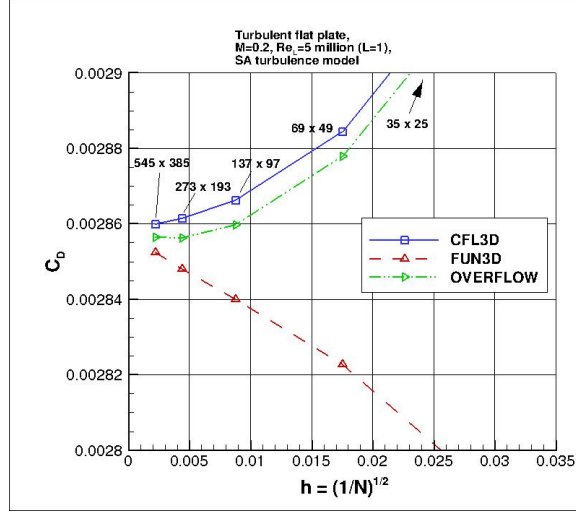

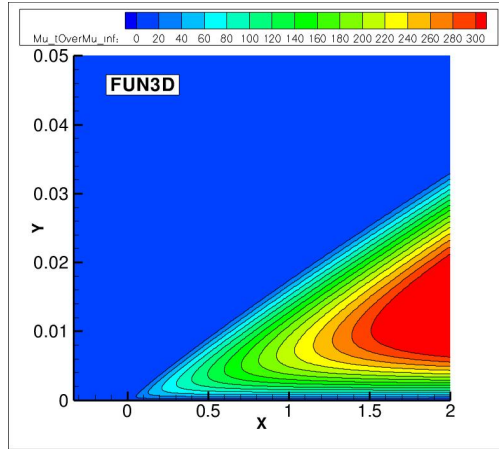Figure 6: SA grid convergence, drag coefficient at $x = 0.97$.

Figure 7 shows the surface skin friction coefficient on the finest 545×385 grid over the entire plate from all three codes. The three codes yield nearly identical results over the plate and the skin friction curves plot on top of one another.

The eddy viscosity contours, nondimensionalized by freestream laminar viscosity, from the three codes on the finest 545×385 grid, are shown in Figure 8 (y-scale expanded for clarity).

Again, using the finest 545×385 grid, an extracted nondimensional eddy viscosity profile at $x = 0.97$ is shown in Figure 9, along with a plot of the maximum nondimensional eddy viscosity as a function of x. The results from the three codes plot on top of one another.

In terms of inner wall variables u^+ and y^+, the finest grid yields the results in Figure 10, which shows the two x-locations $x = 0.97008$ and $x = 1.90334$. The law-of-the-wall theory with $\kappa = 0.41$ and $B = 5.0$ is also shown [9].

Standard velocity profiles are shown for the finest grid at the same two x-locations x=0.97008 and x=1.90334 in Figure 11.

8
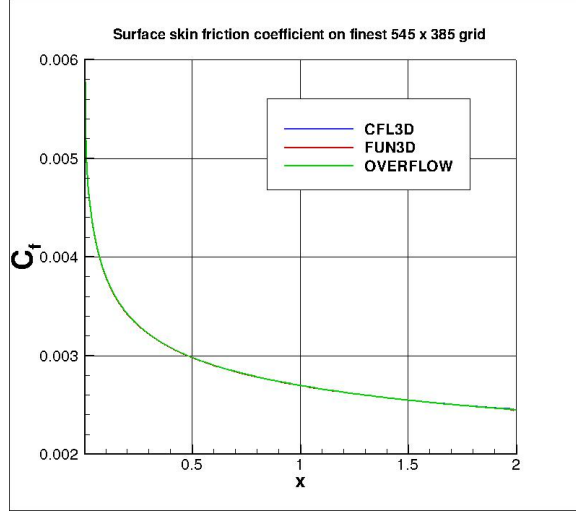
Figure 7: SA C_f as a function of x.

2.2 Overflow Flate Plate SST-V Results

By default, OVERFLOW uses second-order accurate spatial differencing for convection in the SST and SST-V flat plate turbulence models. We discovered that in some cases a better comparison with CFL3D and FUN3D comes from using first-order differencing for the SST/SST-V convection terms. Here we show the first-order OVERFLOW results.

Figure 12 shows residual history convergence characteristics and turbulence residual history convergence for the different grid refinements for OVERFLOW run with first-order differencing for turbulence convection terms. All residuals converged to machine zero.

Figure 13 shows the drag coefficient for each of the three codes on the four finer grids. For each code, the drag coefficient is convergent as the grid is refined, and the codes are consistent with one another.

Figure 14 shows the convergence of the wall skin friction coefficient at $x = 0.97008$, as a function of grid size for the three codes. As can be seen, all three codes give approximately the same result as the grid is refined.

Figure 15 shows the convergence of the drag coefficient at $x = 0.97008$ as a function of grid size for the three codes. The drag coefficient is convergent as the grid is refined, and the three codes are consistent with one another.

9
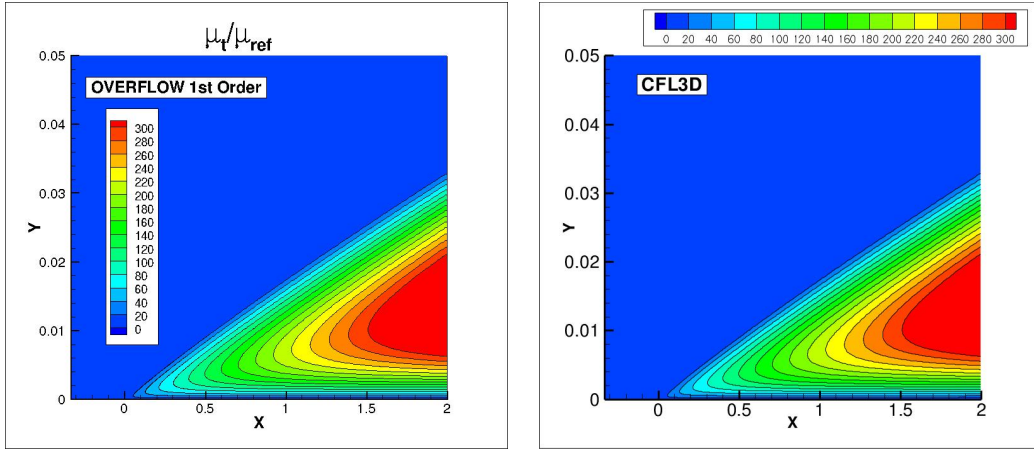
(a) OVERFLOW

(b) CFL3D

(c) FUN3D

Figure 8: SA eddy viscosity contours, finest grid.

(a) Eddy viscosity profile in y at $x = 0.97$ (b) maximum eddy viscosity in x
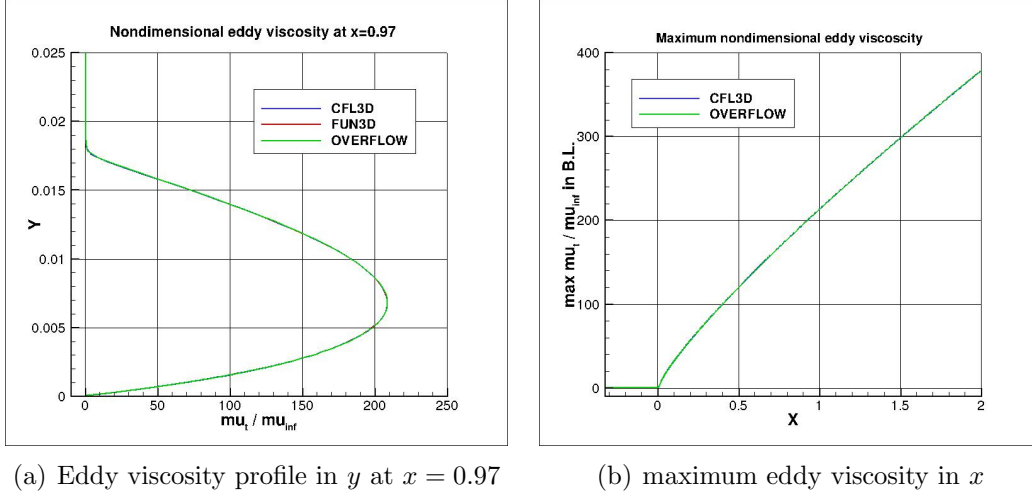
Figure 9: SA eddy viscosity distributions.
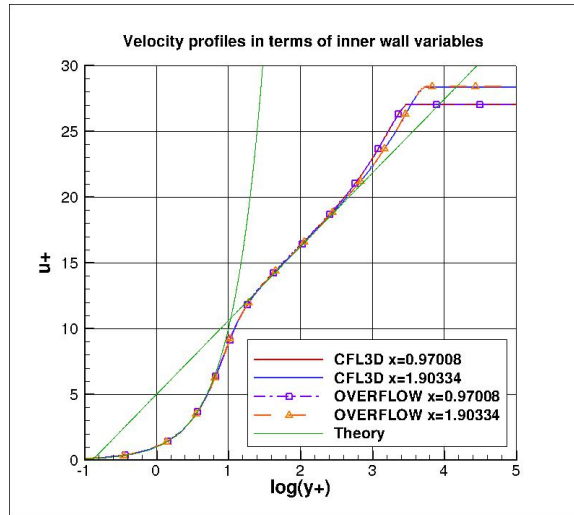
Figure 10: SA velocity profile comparisons: wall variables.

11
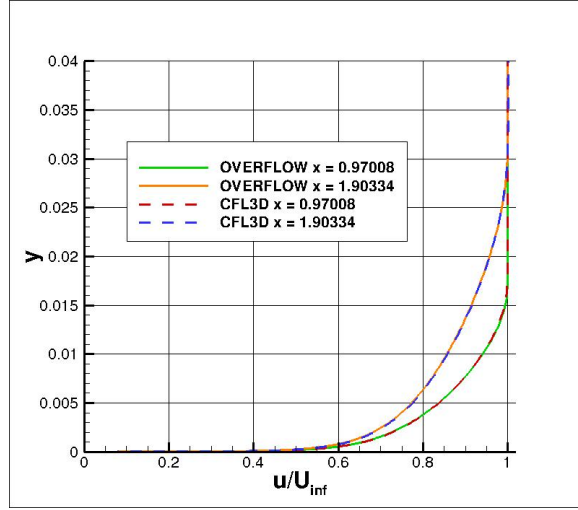
Figure 11: SA velocity profiles at $x = 0.97$ and $x = 1.90$.
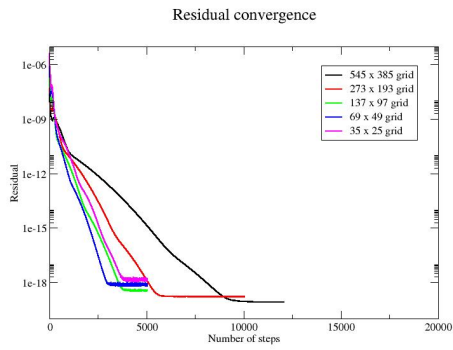
(a) Flow solver residual convergence
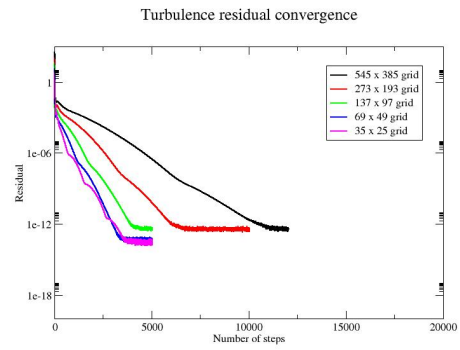
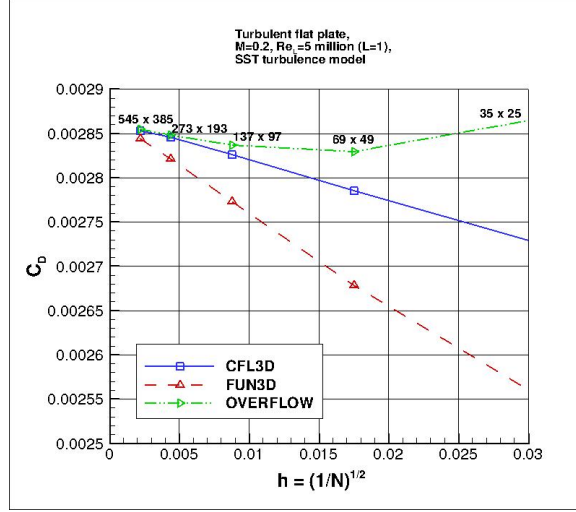(b) Turbulence model convergence

Figure 12: SST-V convergence characteristics, flat plate.

12

Figure 13: SST-V drag convergence, flat plate.
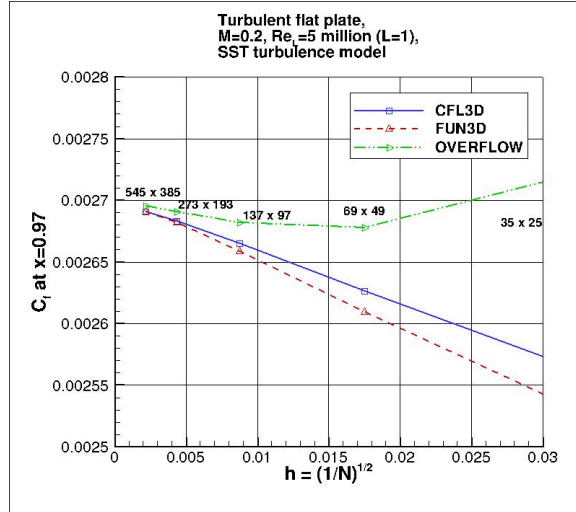
Figure 14: SST-V wall skin friction grid convergence, C_f at $x = 0.97$.
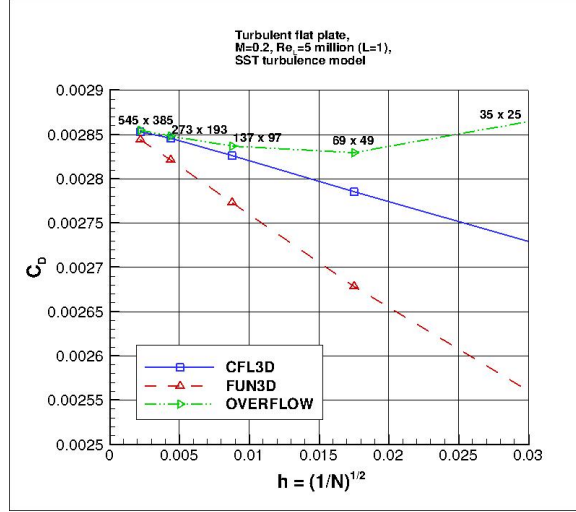
Figure 15: SST-V grid convergence, drag coefficient at $x = 0.97$.

The surface skin friction coefficient from all three codes on the finest 545×385 grid over the entire plate is shown in Figure 16. The three codes yield nearly identical results over most of the plate.

The nondimensionalized eddy viscosity contours (Figure 17), k contours (Figure 18), and ω contours (Figure 19) from the three codes on the finest 545×385 grid are shown, (y-scale expanded for clarity). Results from the three codes on this grid are essentially indistinguishable.

Using the finest 545×385 grid, an extracted nondimensional eddy viscosity profile at $x = 0.97$ is shown in Figure 20a, and a plot of the maximum nondimensional eddy viscosity as a function of x is shown in Figure 20b.

Notice that the nondimensional eddy viscosity above has a small "bump" near $y = 0.01$ in Figure 20. The same behavior occurs for CFL3D, FUN3D, and OVERFLOW on the finest grid. This behavior is due to the SST blending between ω and vorticity in the denominator of the equation for eddy viscosity, and is only noticeable on extremely fine grids for this flat plate case. The bump is located in the region where the SST/SST-V F1 function is in the process of transitioning from 1 to 0, as shown in Figure 21 from the 545×385 grid.

The nondimensional k and ω profiles at $x = 0.97008$ from the 545×385 grid are shown in figures 22a and 22b.

14
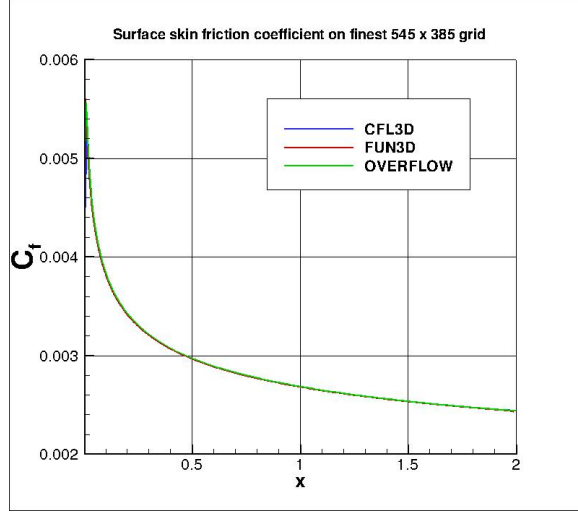
Figure 16: SST-V C_f as a function of x.

In terms of inner wall variables u^+ and y^+, the finest grid yields the results shown in Figure 23, which shows u^+ and y^+ variables at two x-locations $x = 0.97008$ and $x = 1.90334$. The dependence of u^+ on y^+ according to law-of-the-wall theory with $\kappa = 0.41$ and $B = 5.0$ is also shown [9].
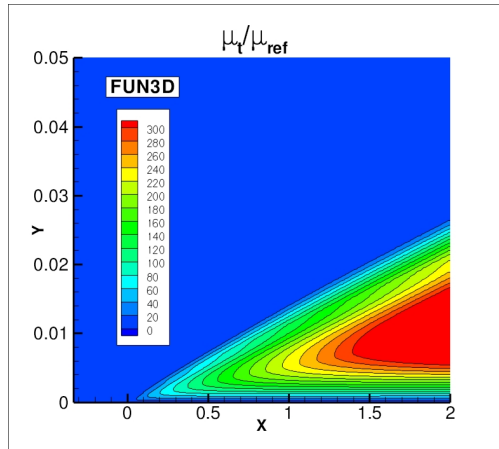
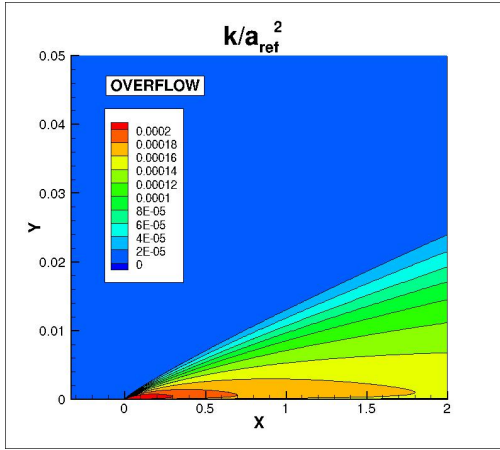Standard velocity profiles are shown for the finest grid at the same two x-locations x=0.97008 and x=1.90334 in Figure 24.
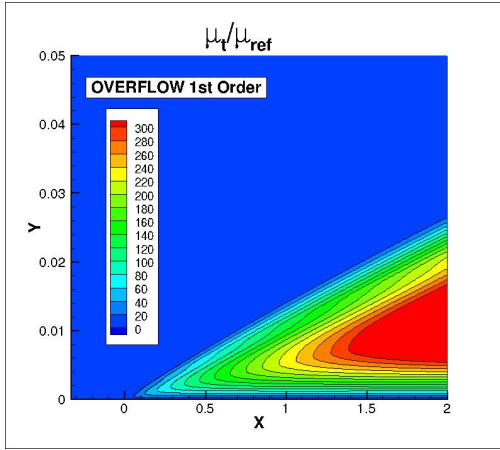
(a) Overflow
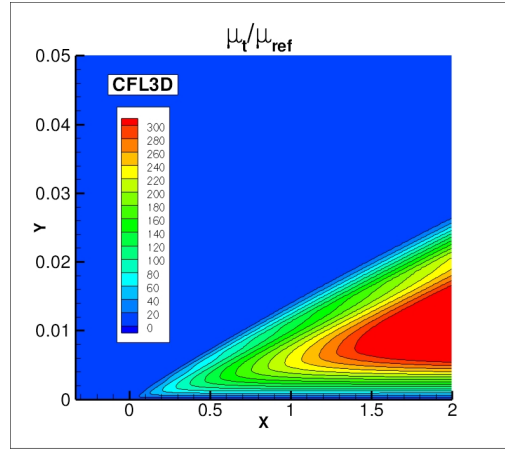
(b) Cfl3d

(c) Fun3d

Figure 17: SST-V eddy viscosity contours, finest grid.
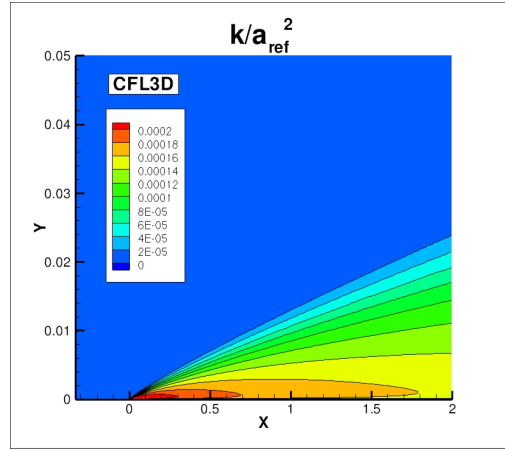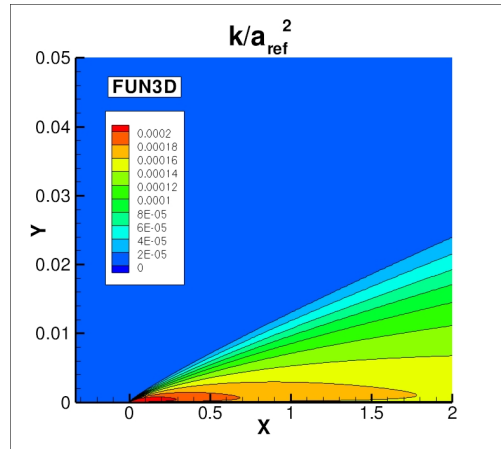
(a) Overflow

(b) Cfl3d

(c) Fun3d

Figure 18: SST-V k contours, finest grid.
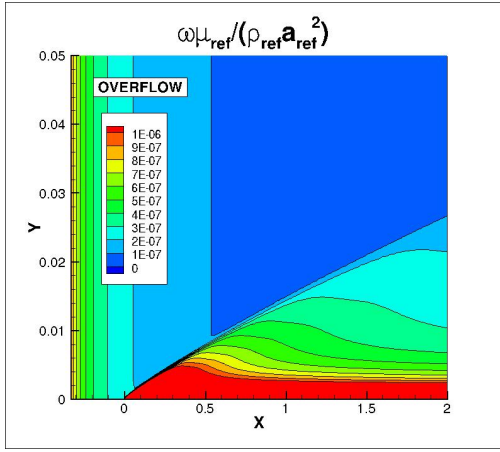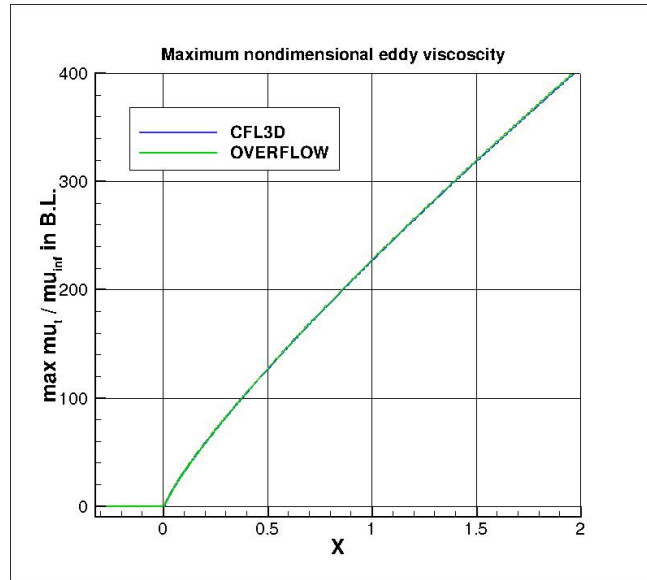
(a) OVERFLOW
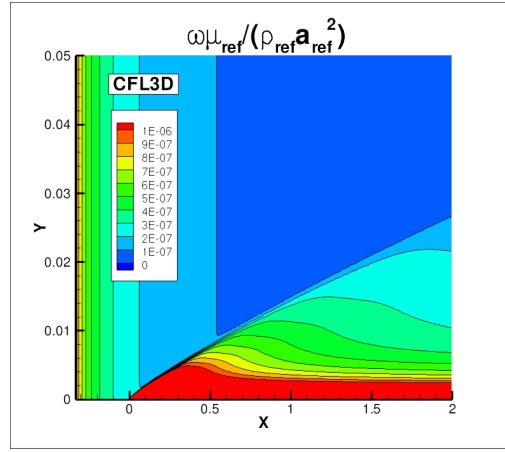
(b) CFL3D
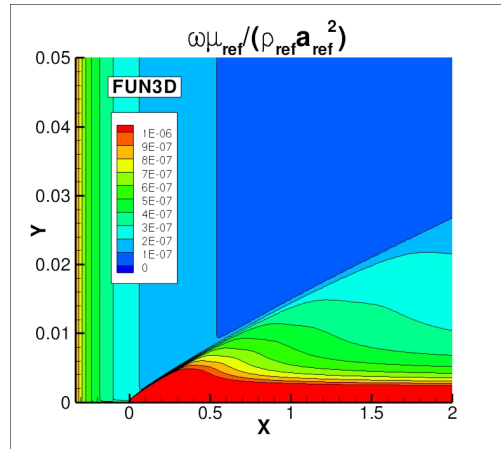
(c) FUN3D

Figure 19: SST-V ω contours, finest grid.
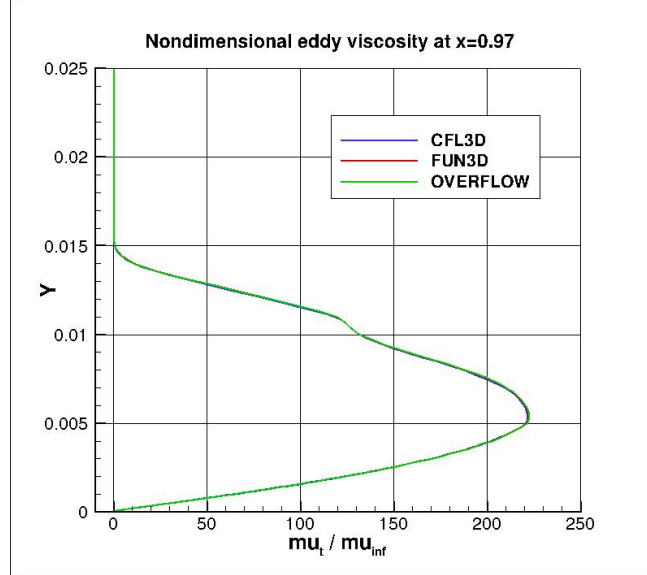
(a) Eddy viscosity profile in y at $x = 0.97$

(b) Max eddy viscosity as a function of x

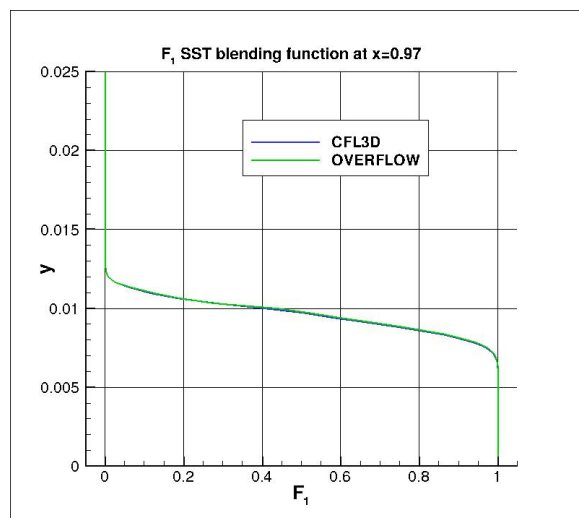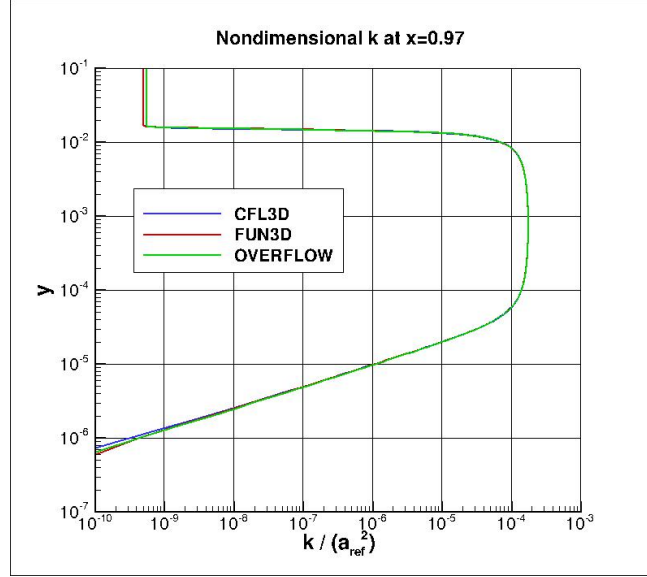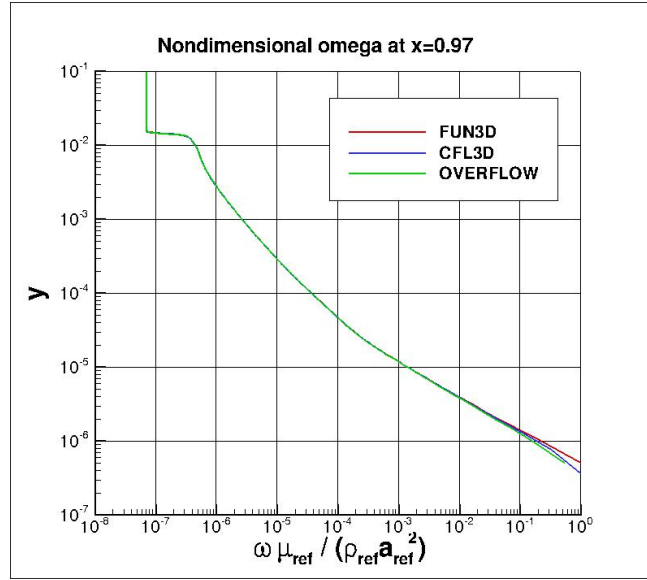Figure 20: SST-V eddy viscosity distributions.

Figure 21: SST-V blending function F1 at $x = 0.97$

(a) k profile in y at $x = 0.97$

(b) ω profile in y at $x = 0.97$

Figure 22: k and ω at $x = 0.97$.

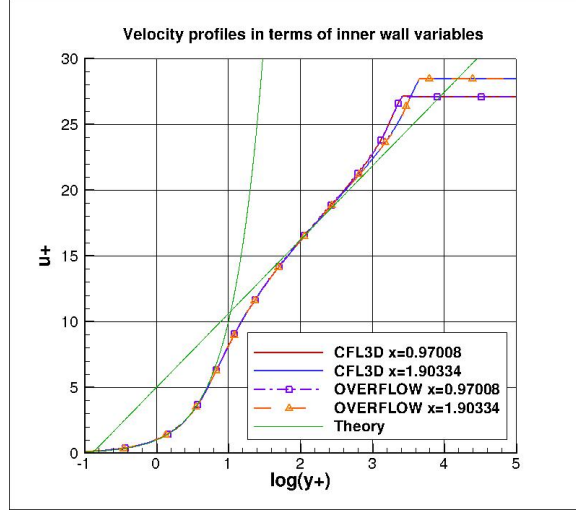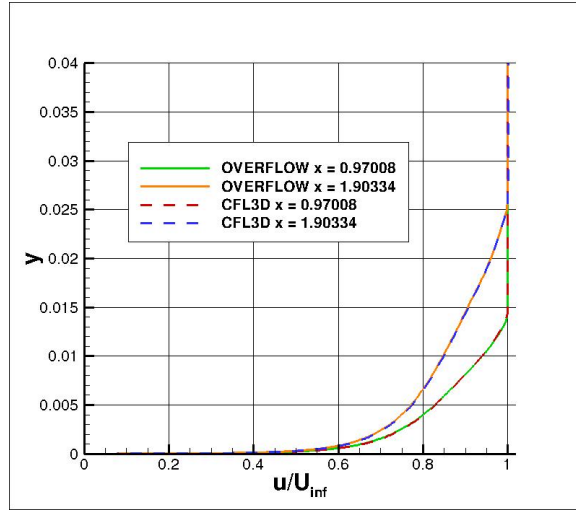Figure 23: SST-V velocity profile comparisons: wall variables.

Figure 24: SST-V velocity profiles at $x = 0.97$ and $x = 1.90$.

3 Planar Shear

In this section we present turbulence model verification for OVERFLOWperformed using the TMR Planar Shear test case. This case focuses on the development of the free shear layer following the passing of two different streams over a thin plate. The narrow, inner stream has a Mach number near $M = 0.5$, while the outer, wider stream has a Mach number near $M = 0.25$. This can also be considered as a planar co-flowing jet [10]. The Reynolds number is $Re = 50000$ based on a grid length of 1. The computational domain is $-10 < x < 200$ and $0 < y < 100$. The separating plate extends from $-10 < x < 0$ at $y = 0.5$. In terms of the plate, the reference length is 10 units. Both the lower and upper boundaries are taken to be symmetry planes. Figure 25 shows the layout of this case, along with the boundary conditions. "Pt" denotes total pressure, "P" denotes static pressure, and "Tt" denotes total temperature.

The grids are taken directly from the TMR website[11], which provides details on the formats and other characteristics. Two-dimensional structured grids are the starting point for OVERFLOW. Each of the five grid refinements has 3 zones, with the following dimensions:

- 129×257, 129×257, 513×513 (denoted L0)

- 65×129, 65×129, 257×257 (denoted L1)

- 33×65, 33×65, 129×129 (denoted L2)

- 17×33, 17×33, 65×65 (denoted L3)

- 9×17, 9×17, 33×33 (denoted L4)

For example, Figure 26 shows the L2 grid system.

The TMR website provides expected CFL3D and FUN3D results for the SA and SST-V models.

The grids provided were put into the three-plane two-dimensional form used by OVERFLOW and input files were generated for the cases with appropriate boundary and flow conditions. We used the Roe flux scheme with low-Mach preconditioning.

In order to make this grid system compatible with the OVERFLOW overset methodology, the original structured one-to-one abutting grids were extended to produce a five-point overlap at each non-physical boundary. Two grid
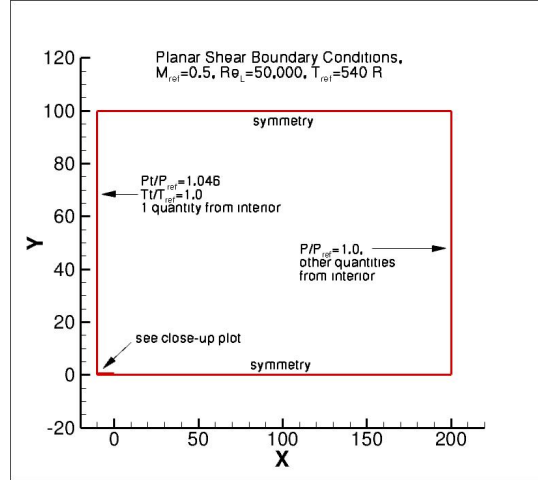
(a) 2D Planar Shear Layer Topology
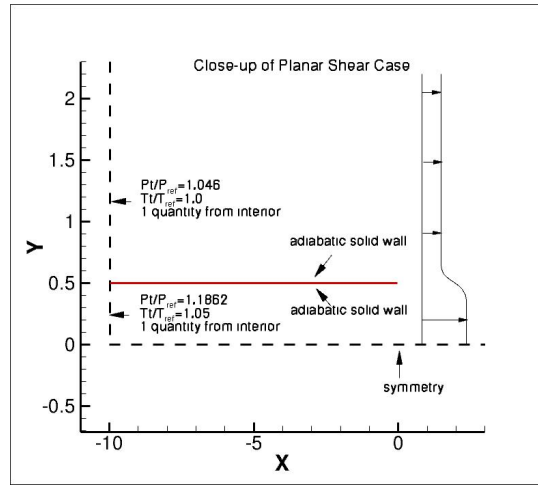
(b) Plate Layout and Conditions

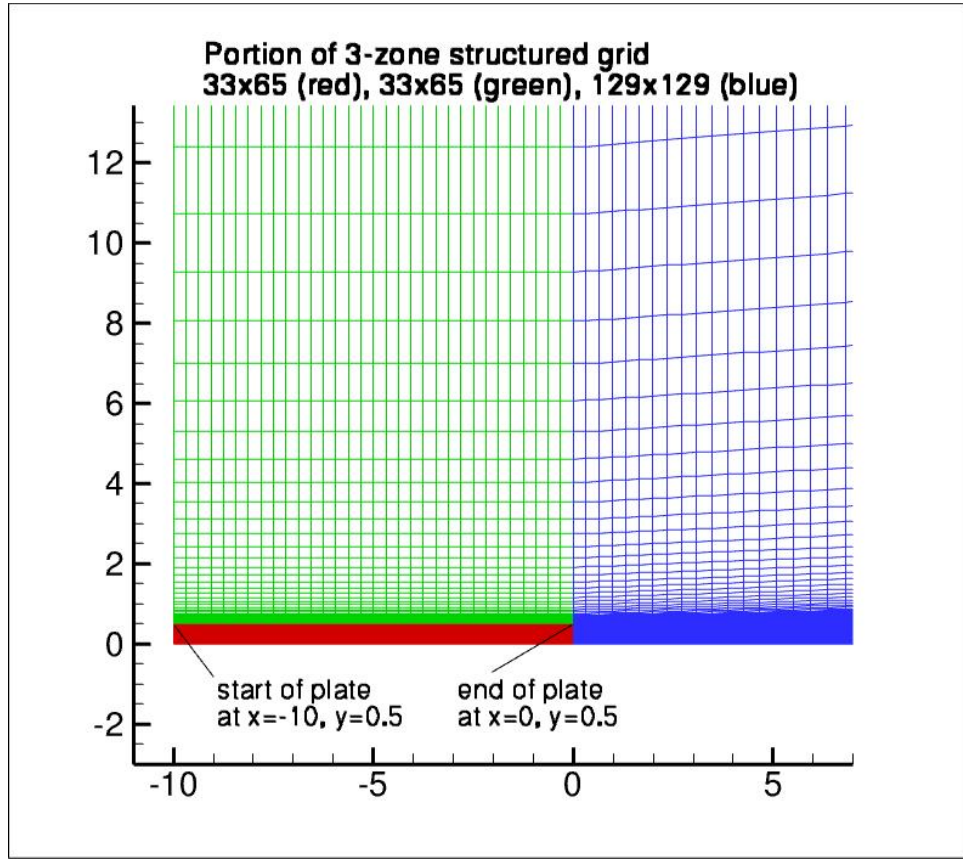Figure 25: Planar shear layer geometry and boundary conditions.

24

Figure 26: Grid system for planar shear layer.

points of the blue grid in Figure 26 were appended to the red and green grids, while two grid points of the red and green grids were prepended to the blue grid. This produces an overset grid system that is appropriate for OVERFLOW.

An OVERFLOW input file for the SA model on the finest grid is shown below:

```
&GLOBAL
    NSTEPS= 40000,  RESTRT= .F.,
    MULTIG= .T.,  FMG   = .T.,  FMGCYC= 100,100,  NGLVL = 2,
    NQT   = 102,
    MAX_GRID_SIZE = 80000,
    /
&OMIGLB
   IRUN  = 0,
   /
&DCFGLB /
&GBRICK
   OBGRIDS= .F.,
   /
&BRKINP /
&GROUPS /

&FLOINP
    FSMACH= 0.5,  REY   = 5.E4,  MUTINF = 0.2,
    /
&VARGAM /

&GRDNAM
    NAME  = 'TMR Planar Shear SA Zone 1',
    /
&NITERS /
&METPRM
    IRHS = 4,
    /
&TIMACU
    DT    = 1.0,  CFLMIN= 10,
    /
```

```
&SMOACU
    DIS2  = 10,  DIS4  = 0.2,  FSO = 3,
    /
&VISINP
    CFLT  = 4,
    /
&BCINP
    IBTYP = 17,  5, 41, 21,
    IBDIR =  2, -2,  1,  3,
    JBCS  =  1,  1,  1,  1,
    JBCE  = -3, -3,  1, -1,
    KBCS  =  1, -1,  1,  1,
    KBCE  =  1, -1, -2, -1,
    LBCS  =  2,  2,  2,  1,
    LBCE  = -2, -2, -2,  1,
    BCPAR1(3) = 1.0, BCPAR2(3) = 1.0,
    /
&SCEINP /
&SIXINP
    /

&GRDNAM
    NAME  = 'TMR Planar Shear SA Zone 2',
    /
&NITERS /
&METPRM
    /
&TIMACU
    /
&SMOACU
    /
&VISINP
    /
&BCINP
    IBTYP =  5, 17, 41, 21,
    IBDIR =  2, -2,  1,  3,
    JBCS  =  1,  1,  1,  1,
    JBCE  = -3, -3,  1, -1,
```

```
    KBCS  =  1, -1,  2,  1,
    KBCE  =  1, -1, -1, -1,
    LBCS  =  2,  2,  2,  1,
    LBCE  = -2, -2, -2,  1,
    BCPAR1(3) = 0.881798, BCPAR2(3) = 0.9523209,
    /
&SCEINP /
&SIXINP
    /


&GRDNAM
    NAME  = 'TMR Planar Shear SA Zone 3',
    /
&NITERS /
&METPRM
    /
&TIMACU
    /
&SMOACU
    /
&VISINP
    /
&BCINP
    IBTYP = 17,   17,   33, 21,
    IBDIR =  2,   -2,   -1,  3,
    JBCS  =  3,    3,   -1,  1,
    JBCE  = -1,   -1,   -1, -1,
    KBCS  =  1,   -1,    1,  1,
    KBCE  =  1,   -1,   -1, -1,
    LBCS  =  2,    2,    2,  1,
    LBCE  = -2,   -2,   -2,  1,
    BCPAR1(3) = 1.0,
    /
&SCEINP /
&SIXINP
    /
```

3.1 Overflow Planar Shear SA Results

Convergence histories for the flow equations and for the turbulence model are shown in Figure 27, where we strove to reach machine zero whenever possible. For all levels of refinement, the flow and turbulence residuals are at or nearly at machine zero.

(a) Flow Solver Residual Convergence   (b) Turbulence Model Convergence
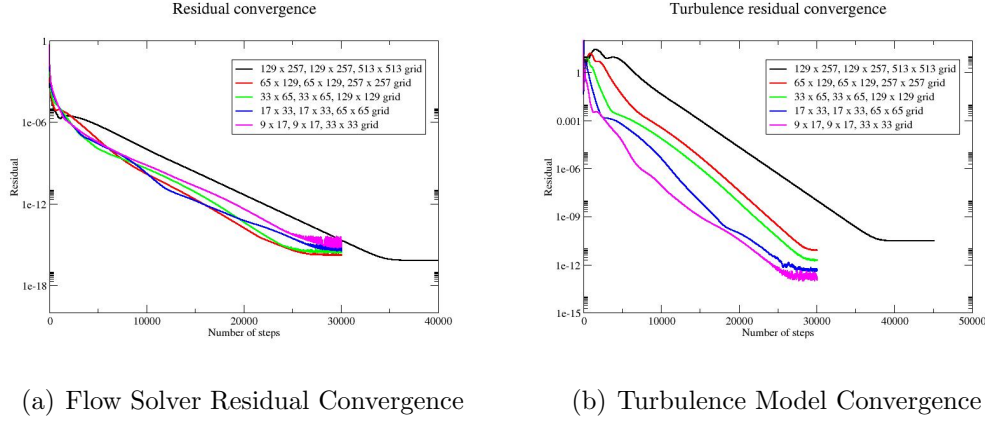
Figure 27: SA convergence characteristics, planar shear.

Figure 28 show a plot of total drag coefficient history for the finest grid for OVERFLOW. The drag coefficient stabilizes to 0.01 counts by step 10,000.

For the CFL3D and FUN3D tests reported here, the turbulent inflow boundary condition used for SA was $\widehat{\nu}_{farfield} = 3\nu_\infty$. For OVERFLOW the freestream eddy viscosity was set to 0.2, which is consistent with the CFL3D and FUN3D results.

Figure 29 shows convergence of the drag coefficient due to skin friction on both sides of the thin plate between $-10 < x < 0$ as a function of grid size for the three codes. In the plot the x-coordinate is $1/N^{\frac{1}{2}}$, which is proportional to grid spacing h. At the left of the plot, $h = 0$ represents an infinitely fine grid. The three codes approach approximately the same result on an infinitely refined grid.

Figure 30 shows convergence of u-velocity (nondimensionalized by the reference speed of sound) at three different locations in the jet: (a) $x = 2.71623$, (b) $x = 29.2468$, and (c) $x = 95.501$. Convergence for the three codes and the two larger values of x is clear, while for OVERFLOW and the
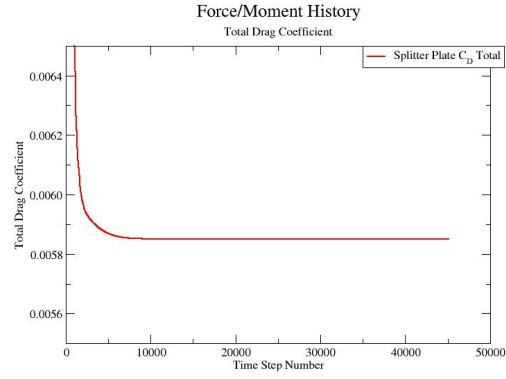
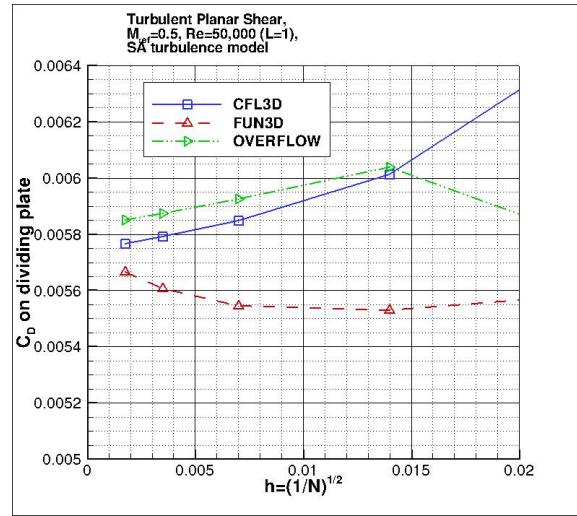Figure 28: SA drag convergence, planar shear.

Figure 29: SA grid convergence, drag coefficient on dividing plate.

smallest value of x, the existence of a converged value, as h is extrapolated to 0, is less clear.

(a) $x = 2.71623$, $y = 0$
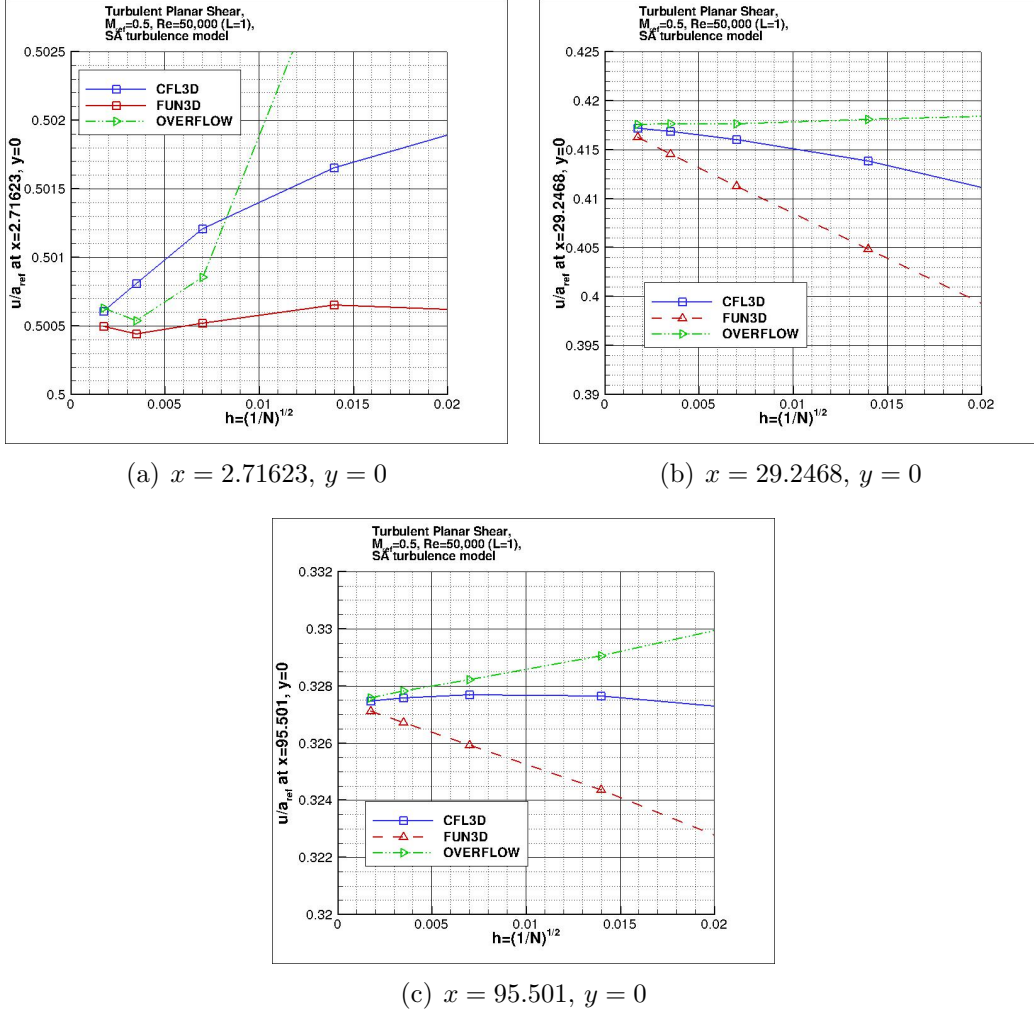
(b) $x = 29.2468$, $y = 0$

(c) $x = 95.501$, $y = 0$

Figure 30: SA grid convergence, u-velocity.

The u-velocity as a function of x at $y = 0$ from the three codes on the finest grid is shown in Figure 31. The plots for the three codes lie atop one another at this scale.

The u-velocity along y at three x-stations from the codes on the finest grid is shown in Figure 32. The plots for the three codes lie atop one another

31
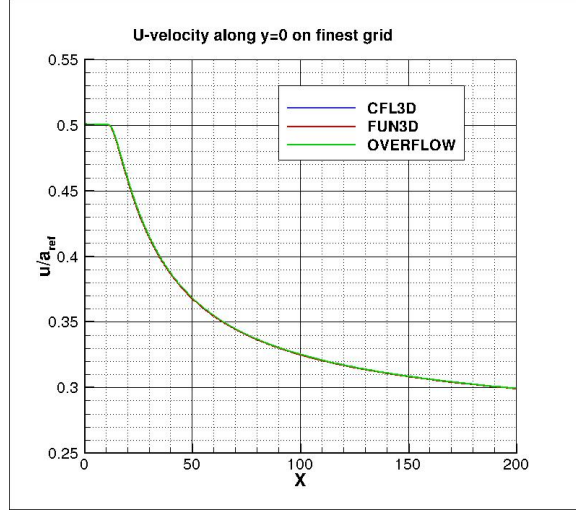
Figure 31: SA u-velocity along $y = 0$.

at this scale.

The eddy viscosity contours (nondimensionalized by freestream laminar viscosity) from the three codes on the finest grid are shown in Figure 33 (y-scale expanded for clarity). The first set of contours (figures 33a-c), are in the far field, and the second set (figures 33d-f), are near the thin plate. The plots for the three codes are essentially the same.

On the finest grid, an extracted nondimensional eddy viscosity profile at $x = 29.2468$ is shown in Figure 34. The OVERFLOW curve is very slightly displaced from the CFL3D and FUN3D curves.

3.2   Overflow SST-V Results

Figure 35 shows convergence of residuals for the flow solver and the turbulence model for the different grid refinements. All cases converged to machine zero.

Figure 36 shows the drag coefficient history on the finest 545×385 grid for OVERFLOW. The drag coefficient stabilizes to 0.01 counts by step 13,000.

Figure 37 shows the convergence of the drag coefficient due to skin friction on both sides of the thin plate between $-10 < x < 0$ as a function of grid size for the three codes. As can be seen, all three codes produce approximately

32
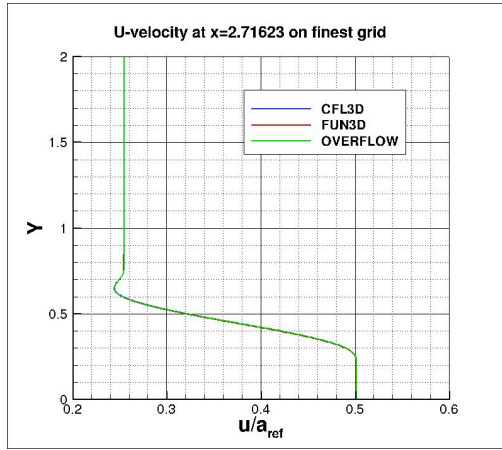
(a) $x = 2.71623, y = 0$
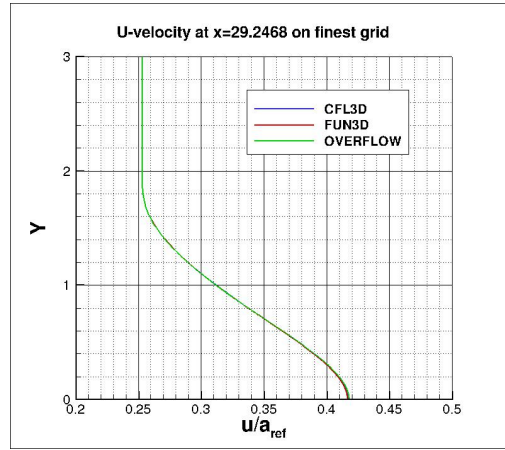
(b) $x = 29.2468, y = 0$
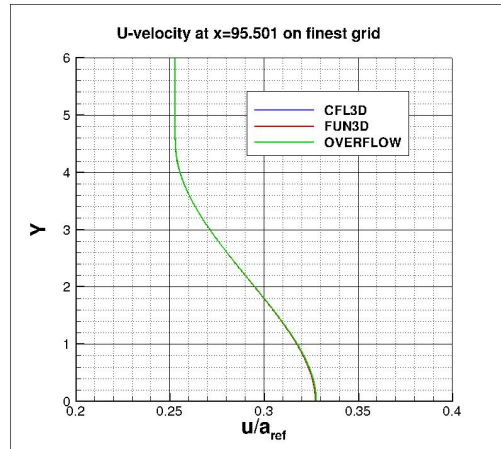
(c) $x = 95.501, y = 0$

Figure 32: SA u-velocity.

(a) Overflow (b) Cfl3d (c) Fun3d
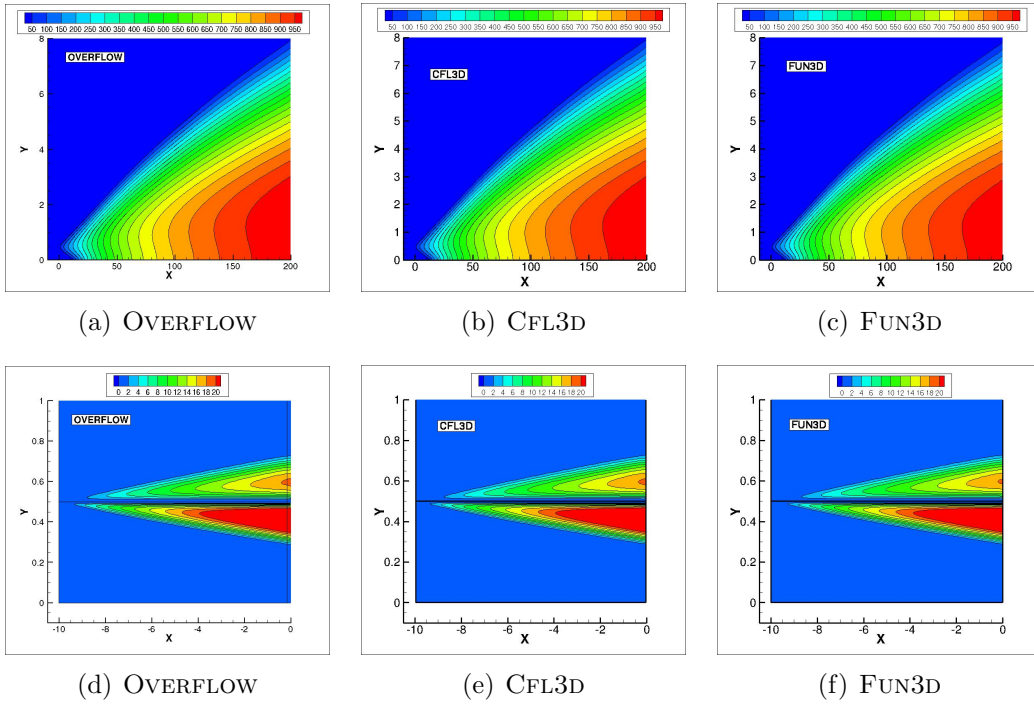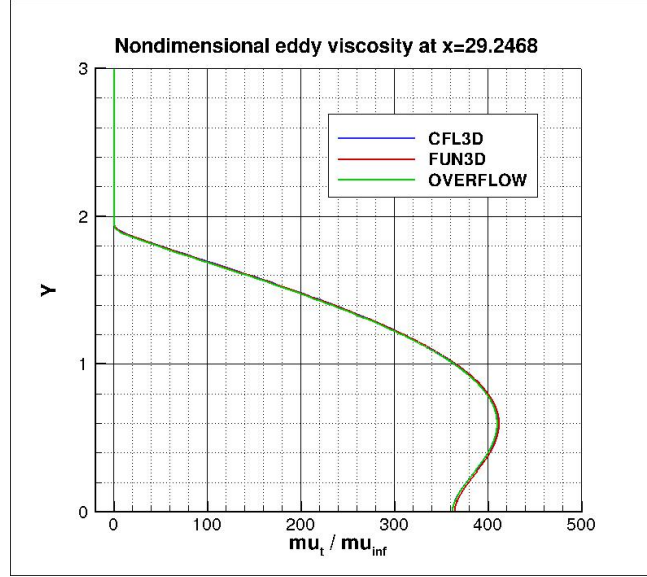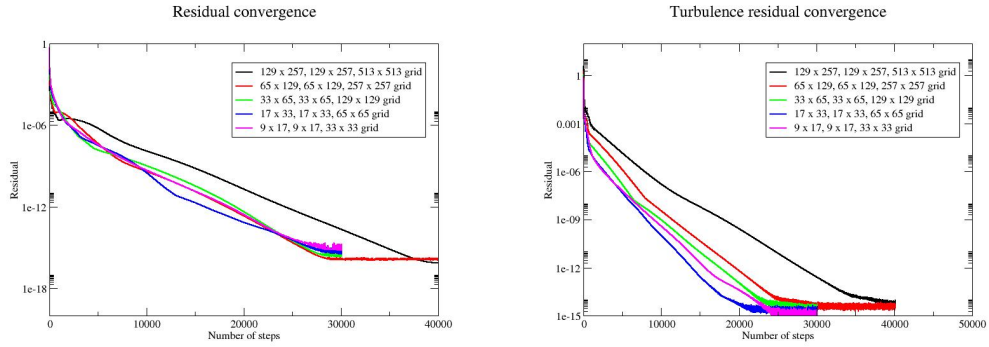
(d) Overflow (e) Cfl3d (f) Fun3d

Figure 33: SA eddy viscosity contours, finest grid.

(a) Eddy Viscosity Profile at $x = 29.2468$

Figure 34: Eddy Viscosity Distributions, SA

(a) Flow Solver Residual Convergence

(b) Turbulence Model Convergence

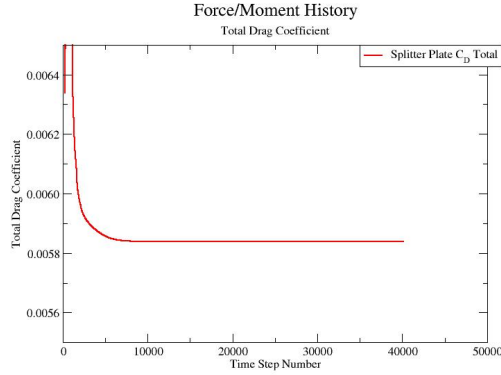Figure 35: SST-V convergence characteristics, planar shear.

Figure 36: SST-V drag convergence, planar shear.

the same result as the grid is refined.

Figure 38 shows u-velocity (nondimensionalized by reference speed of sound) at 3 different locations in the jet: (a) $x = 2.71623$, (b) $x = 29.2468$, and (c) $x = 95.501$. For each value of x, the u-velocities on the finest grid produced by the three codes are very close to one another.

Figure 39 shows the u-velocity as a function of x at $y = 0$ from the three codes on the finest grid. At this scale, the curves from the three codes plot atop one another.

The u-velocity as a function of y at three x-stations from the codes on the finest grid is shown in Figure 40. At this scale, the curves from the three codes plot atop one another.

The eddy viscosity contours (nondimensionalized by freestream laminar viscosity) from the three codes on the finest grid are shown in the next set of plots (y-scale expanded for clarity). The first set of contours, (figures 41a-c), are in the far field, and the second set (figures 41d-f), are near the thin plate. In all cases, the contour plots of the three codes are very similar to one another.

The nondimensionalized k and ω contours from the three codes on the finest grid in the far field are shown in Figure 42 (y-scale expanded for clarity). The contour plots of the codes are very similar to one another.

Using the finest grid, extracted nondimensional eddy viscosity (Figure 43a), k (Figure 43b), and ω (Figure 43c) profiles at $x = 29.2468$ are shown. The
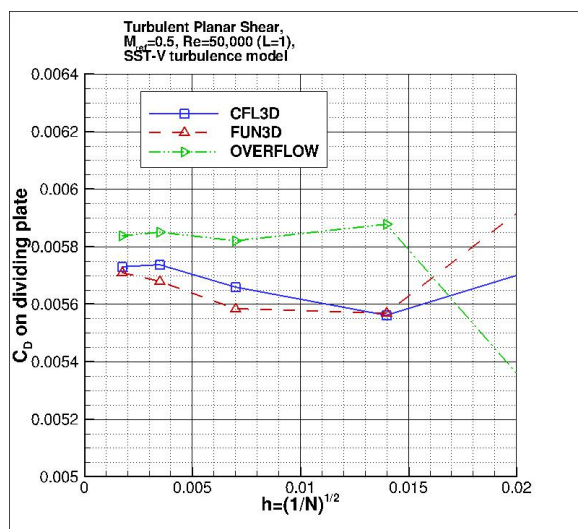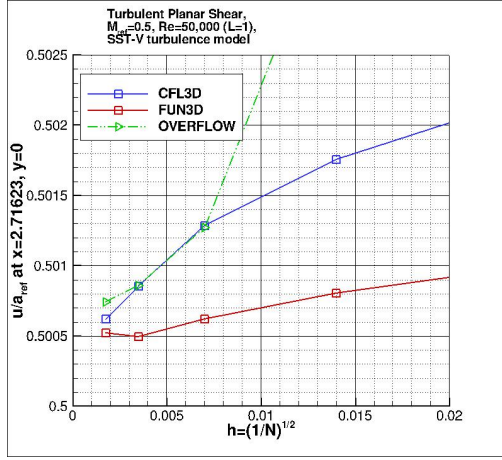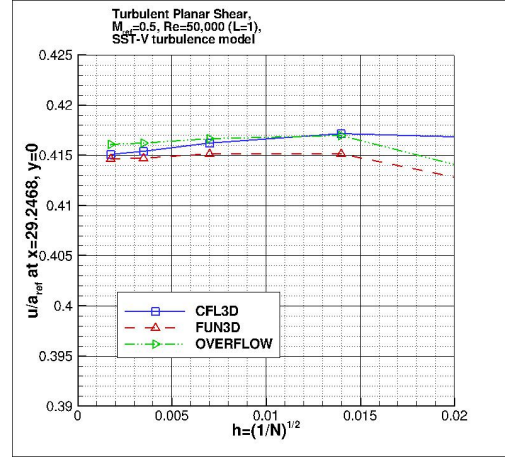
36
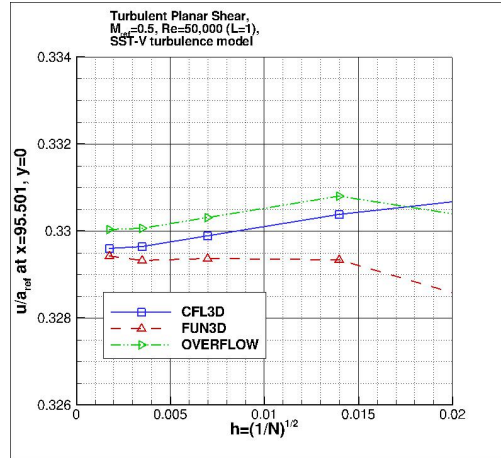
Figure 37: SST-V grid convergence, drag coefficient.

OVERFLOW results are slightly displaced from the CFL3D and FUN3D results.

(a) $x = 2.71623$, $y = 0$

(b) $x = 29.2468$, $y = 0$

(c) $x = 95.501$, $y = 0$
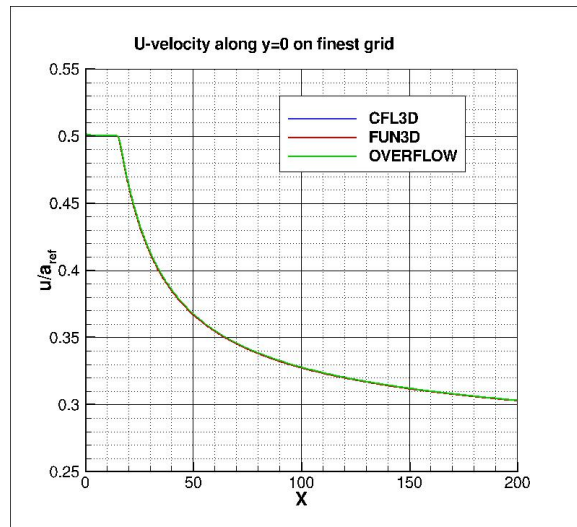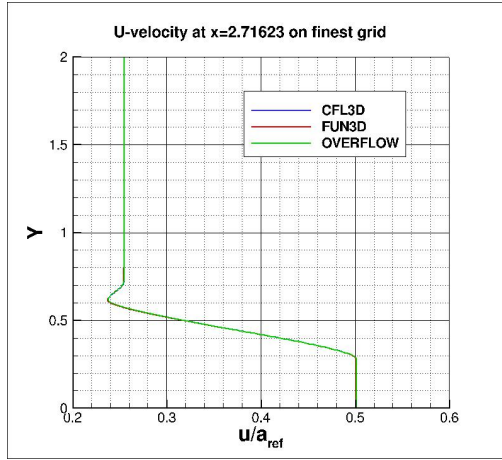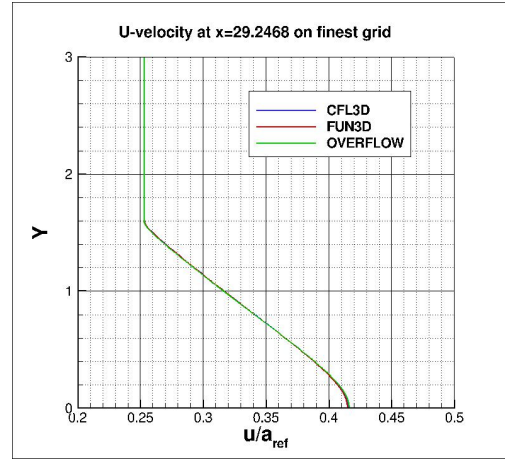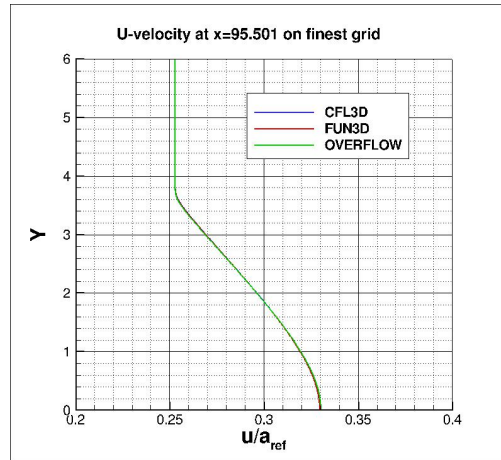
Figure 38: SST-V grid convergence, u-velocity.

Figure 39: SST-V u-velocity along y = 0.

(a) $x = 2.71623$, $y = 0$

(b) $x = 29.2468$, $y = 0$

(c) $x = 95.501$, $y = 0$
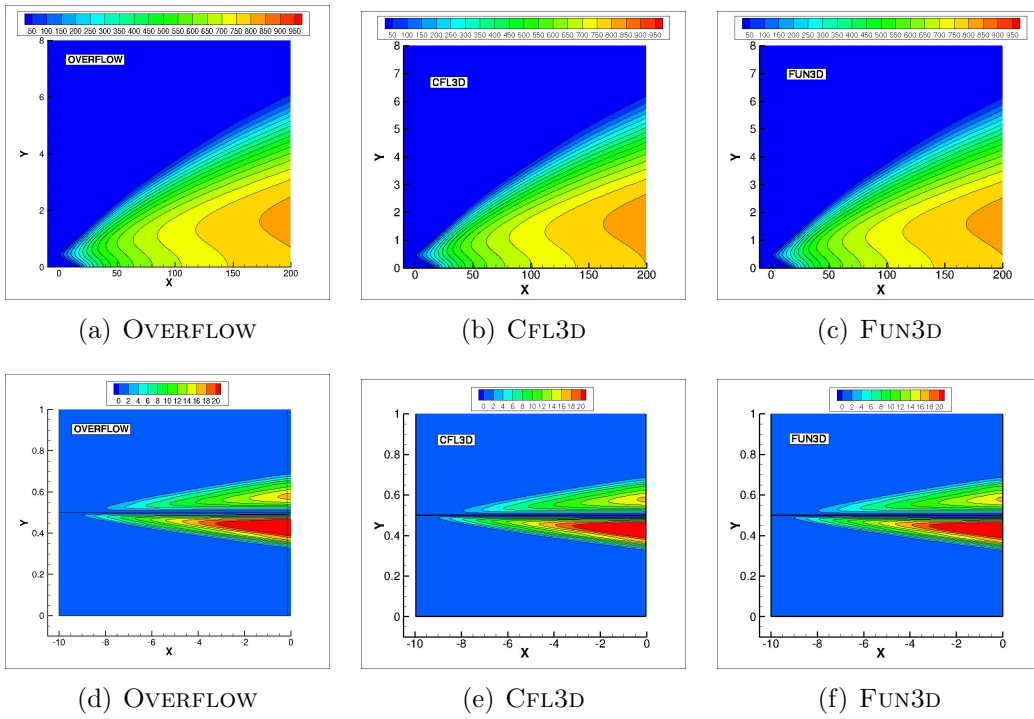
Figure 40: SST-V u-velocity.

(a) OVERFLOW   (b) CFL3D   (c) FUN3D

(d) OVERFLOW   (e) CFL3D   (f) FUN3D

Figure 41: SST-V eddy viscosity contours, finest grid.

(a) k: Overflow   (b) k: Cfl3d   (c) k: Fun3d

(d) ω: Overflow   (e) ω: Cfl3d   (f) ω: Fun3d
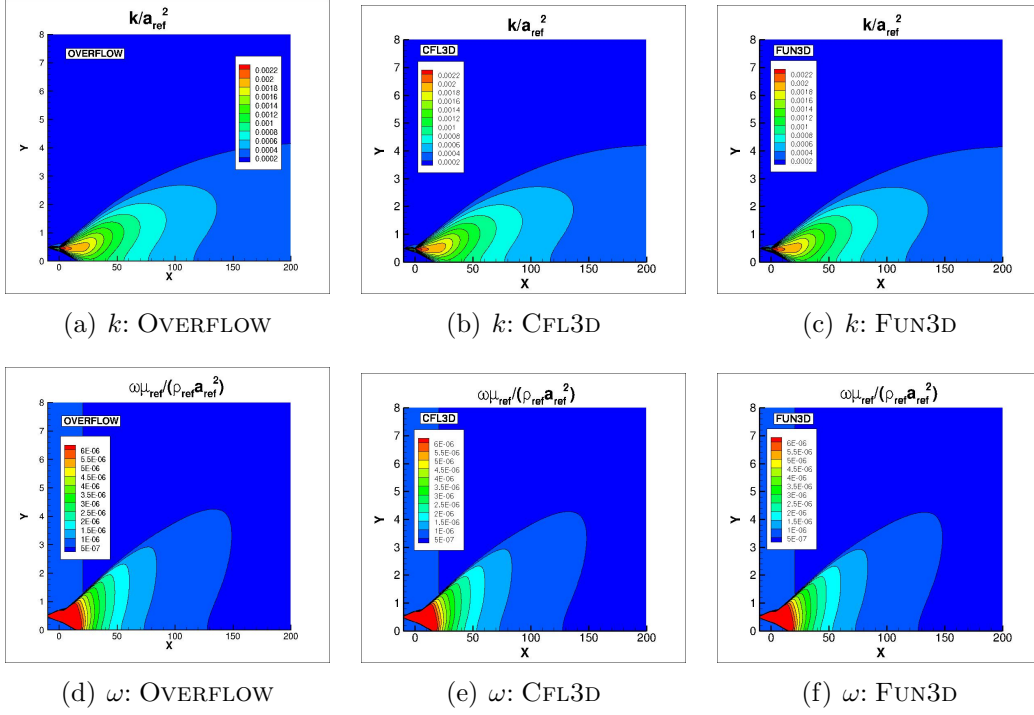
Figure 42: SST-V k and ω contours, finest grid.
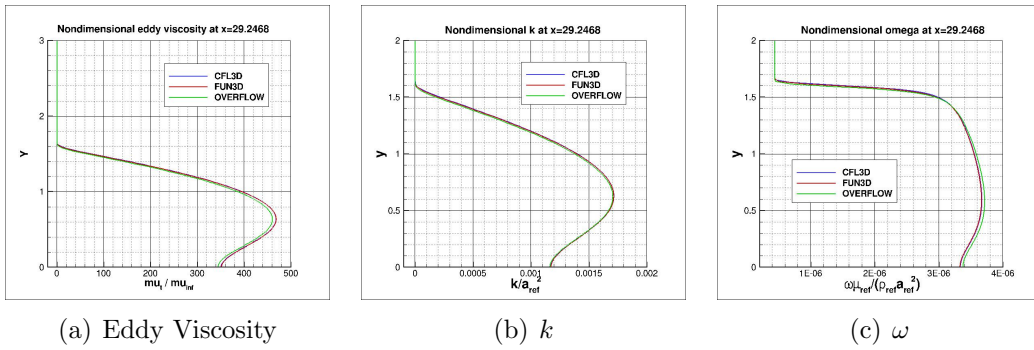

(a) Eddy Viscosity   (b) k (c) ω

Figure 43: Profiles of turbulence quantities at $x = 29.2468$, finest grid.

4 2D Bump

In this section, we discuss turbulence model verification for OVERFLOW performed on the TMR 2D Bump-in-channel test case. This case differs from the simpler flat plate verification case because it involves wall curvature and, as a result, pressure gradients. The case was run at Mach number $M = 0.2$ and Reynolds number $Re = 3$ million based on grid length of 1. The body reference length is 1.5 units. The lower wall is a viscous wall extending from $x = 0$ to $x = 1.5$ with a bump; that is, non-zero y – from $x = 0.3$ to $x = 1.2$. The maximum bump height is 0.05. The definition of the bump is: $y = 0.05(\sin(\pi x/0.9 - (\pi/3)))^4$ for $0 \le x \le 1.2$, $y = 0$ for $0 \le x < 0.3$ and $1.2 < x \le 1.5$. The upstream and downstream far-field boundaries extend 25 units from the viscous wall, with symmetry plane boundary conditions imposed on the lower wall between the far field and the solid wall. The upper boundary, at $y = 5.0$, is taken to be a symmetry plane. Figure 44 shows the layout of this case, along with the boundary conditions.

The grids are taken directly from the TMR website[12], where details on the formats and other characteristics are available. Two-dimensional structured grids are defined with the following dimensions:

- 1409×641 (641 points on solid wall, denoted L0)

- 705×321 (321 points on solid wall, denoted L1)

- 353×161 (161 points on solid wall, denoted L2)

- 177×81 (81 points on solid wall, denoted L3)

- 89×41 (41 points on solid wall, denoted L4)

For example, Figure 45 shows a portion of the L3 grid.

The TMR website provides CFL3D and FUN3D results for the SA, SST, and SST-V turbulence models.

The grids provided were put into the three-plane two-dimensional format for OVERFLOW and input files with appropriate boundary and flow conditions were generated. We used the Roe flux scheme with low-Mach preconditioning. A sample input file for OVERFLOW with the SA model on the L0 grid is below.
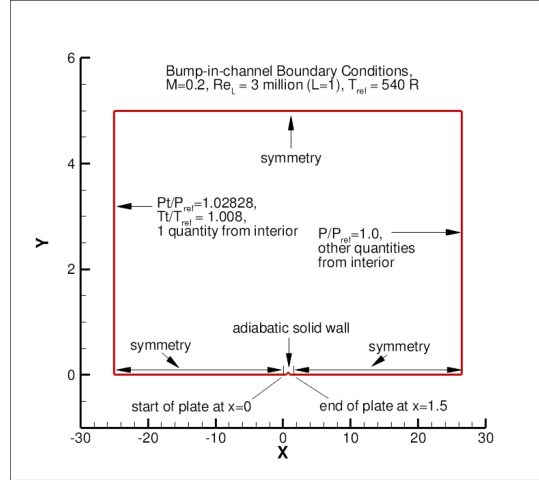
(a) 2D Bump Topology
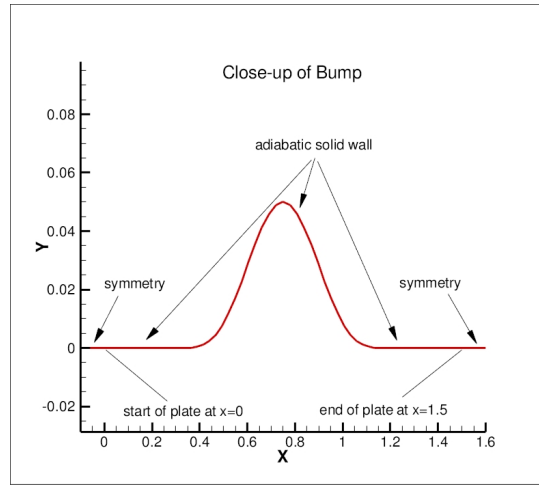
(b) Bump Layout and Conditions

Figure 44: 2D bump geometry and boundary conditions.
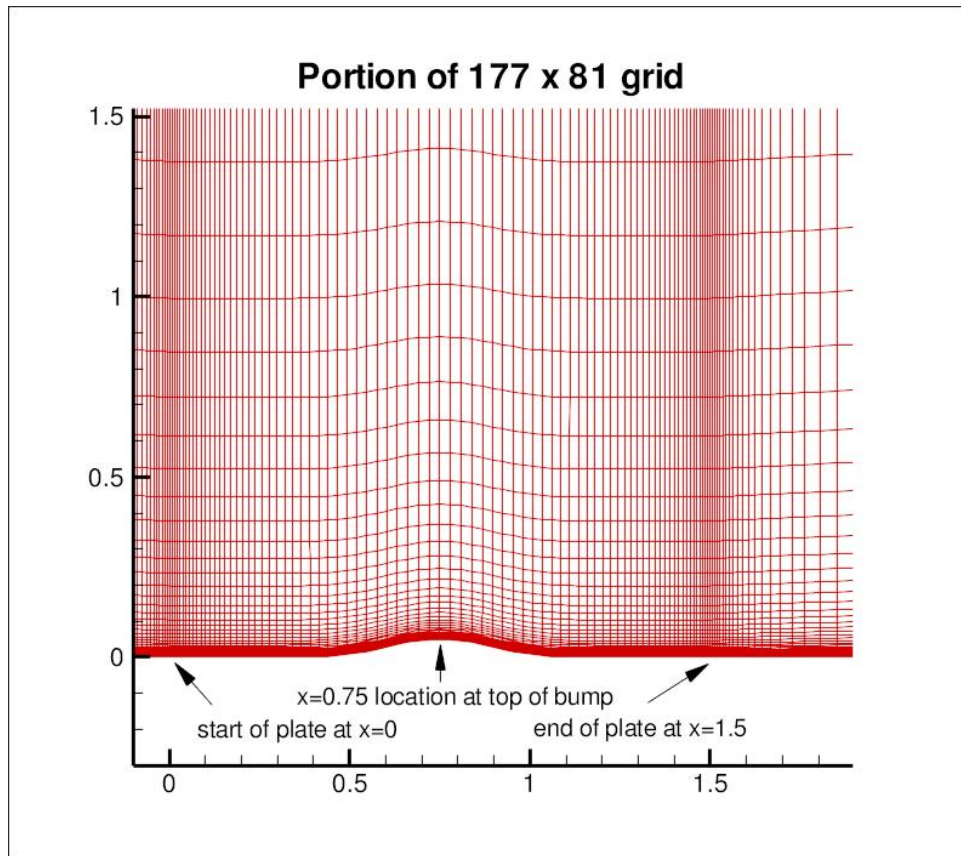
44

Figure 45: Grid system for 2D bump.

```
&GLOBAL
    NSTEPS= 150000,  RESTRT= .F.,
    MULTIG= .T.,  FMG  = .T.,  FMGCYC= 50,50,  NGLVL = 2,
    NQT   = 102,
    /
&FLOINP
    FSMACH= 0.2,  REY   = 3.E6,  MUTINF = 0.2,
    /
&VARGAM /

&GRDNAM
    NAME  = 'TMR 2D Bump SA',
    /
&NITERS /
&METPRM
    IDISS = 4,   BIMIN = -1,
    /
&TIMACU
    DT    = 1.0,  CFLMIN= 25,
    /
&SMOACU
    DIS2  = 0,  DIS4  = 0.01,
    /
&VISINP
    CFLT  = 4,
    /
&BCINP
    IBTYP =  17,    5,  17, 17, 41, 33, 21,
    IBDIR =   2,    2,   2, -2,  1, -1,  3,
    JBCS  =   1, 385,1026,  1,  1, -1,  1,
    JBCE  = 384,1025,  -1, -1,  1, -1, -1,
    KBCS  =   1,   1,   1, -1,  1,  1,  1,
    KBCE  =   1,   1,   1, -1, -1, -1, -1,
    LBCS  =   2,   2,   2,  2,  2,  2,  1,
    LBCE  =  -2,  -2,  -2, -2, -2, -2,  1,
    BCPAR1(5) = 1.0, BCPAR2(5) = 1.0, BCPAR1(6) = 1.0,
    /
&SCEINP /
```

4.1 Overflow SA Results

For the CFL3D and FUN3D test results, reported below, the turbulent inflow boundary condition used for SA was $\widehat{\nu}_{farfield} = 3\nu_\infty$. In OVERFLOW the freestream eddy viscosity was set to 0.2, which is consistent with the CFL3D and FUN3D computations.

Typical OVERFLOW residual convergence histories are shown in Figure 46. For all grids the flow and turbulence residuals have reached machine zero. We attribute the slow convergence of residuals to the singularity in the boundary conditions, because along the bottom wall the boundary condition changes discontinuously from a reflection plane to a viscous wall and then back to a reflection plane. In a calculation not shown here, we found that changing the boundary condition along the bottom boundary to be a viscous wall everywhere greatly improved convergence.

(a) Flow Solver Residual Convergence   (b) Turbulence Model Convergence
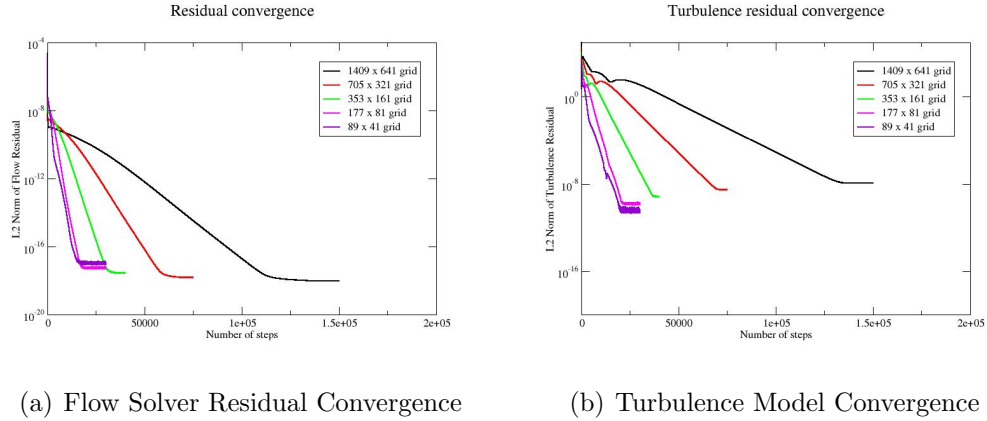
Figure 46: SA convergence characteristics, 2D bump.

Figure 47 shows convergence of total drag, pressure drag, viscous drag, and lift for the finest grid using OVERFLOW. All the forces are well converged.

Figure 48 shows the convergence of the wall skin friction coefficient C_f as a function of grid size at the bump peak ($x = 0.75$), in front of the peak ($x = 0.6321975$), and aft of the peak ($x = 0.8678025$) for the three codes. In the plot the x-coordinate is $1/N^{\frac{1}{2}}$, which is proportional to grid spacing h. The three codes are consistent with one another as the grid is refined.
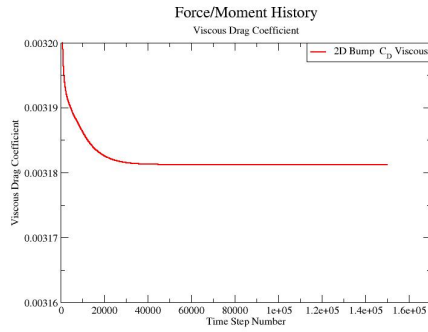
Figure 49 shows: (a) total drag coefficient, (b) pressure drag coefficient, (c) viscous drag coefficient, and (d) total lift coefficient as functions of grid
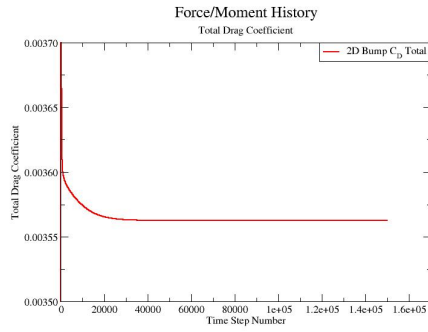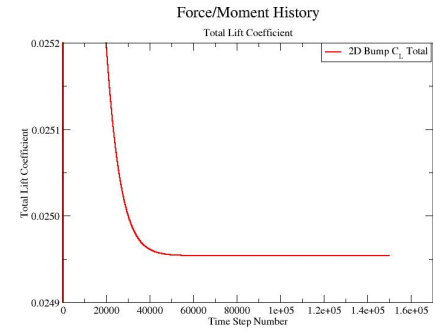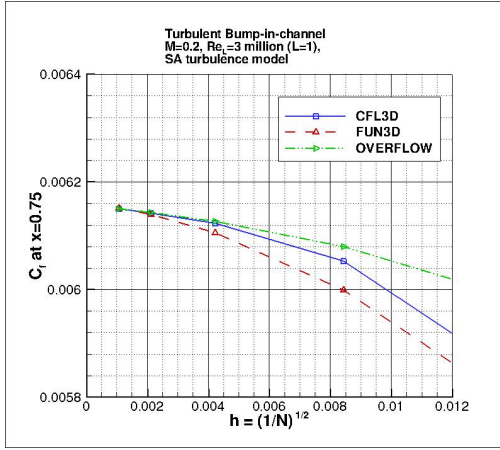
(a) Total Drag
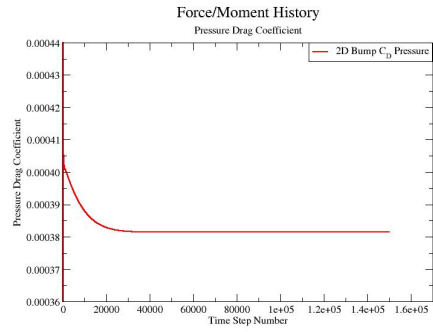
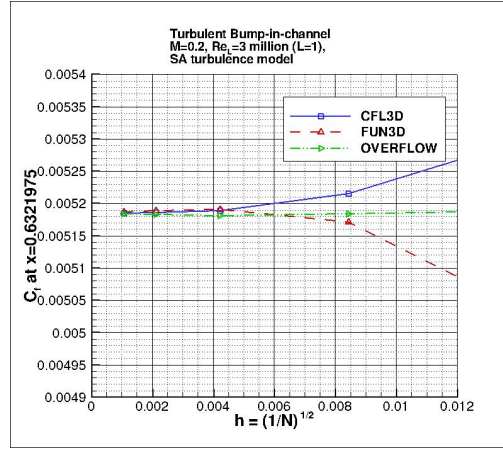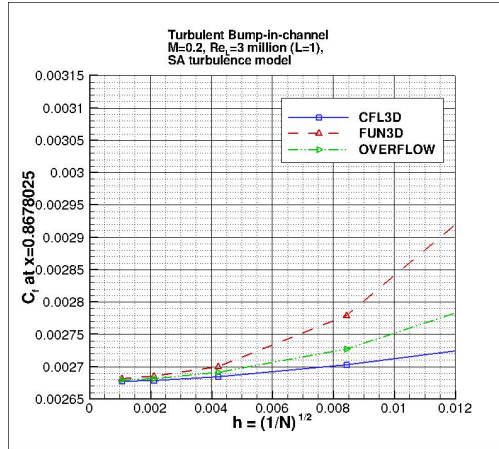(b) Pressure Drag

(c) Viscous Drag

(d) Total Lift

Figure 47: SA loads convergence, 2D bump.

(a) C_f at $x = 0.75$

(b) C_f at $x = 0.632197$

(c) C_f at $x = 0.8678025$

Figure 48: SA skin friction convergence, 2D bump.

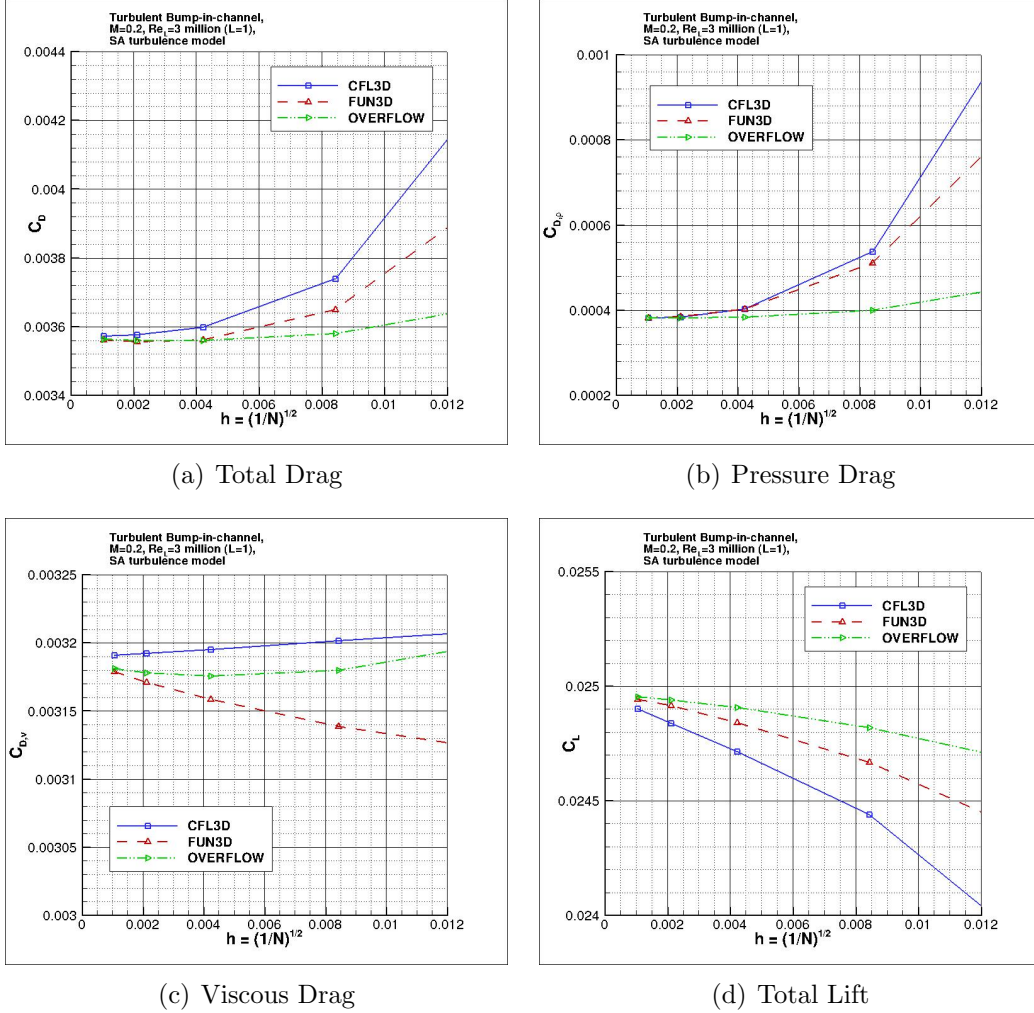size. The three codes appear to be consistent with one another as the grid is refined.

(a) Total Drag

(b) Pressure Drag

(c) Viscous Drag

(d) Total Lift

Figure 49: SA convergence of loads as function of grid size.

The surface skin friction coefficient from all three codes on the L0 1409 × 641 grid, over the entire bump wall, is shown in Figure 50a. The surface pressure coefficient C_p from all three codes on the finest grid, over the entire bump wall, is shown in Figure 50b.

In this bump case, the surface skin friction is singular (tends toward

infinity) at the leading edge. The finer the grid, the more nearly singular the local behavior on a finite grid. Locally anomalous behavior in C_f is also seen at the back end of the bump wall (at $x = 1.5$), similar to that often seen in CFD solutions near trailing edges. Both of these behaviors may have some influence on the convergence of the integrated viscous component of the drag coefficient.
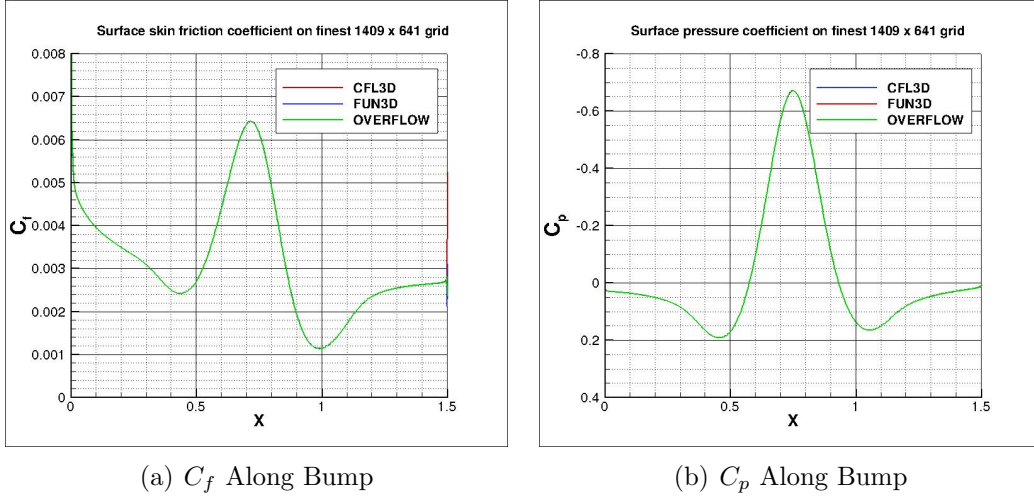

(a) C_f Along Bump

(b) C_p Along Bump

Figure 50: C_f and C_p along bump, finest grid.

The eddy viscosity contours (nondimensionalized by freestream laminar viscosity) from the three codes on the finest 1409×641 grid are shown in Figure 51 (y-scale expanded for clarity). The contour plots for the three codes are very similar.

Using the finest 1409×641 grid, an extracted nondimensional eddy viscosity profile at $x = 0.75$ is shown in Figure 52a, along with a plot of the maximum nondimensional eddy viscosity as a function of x, shown in Figure 52b. The TMR website only provides maximum eddy viscosity for CFL3D, not for FUN3D. The different codes give results that plot atop one another.

Scaled u-velocity profiles at two x locations for OVERFLOW and CFL3D are shown in Figure 53. The curves plot atop one another.
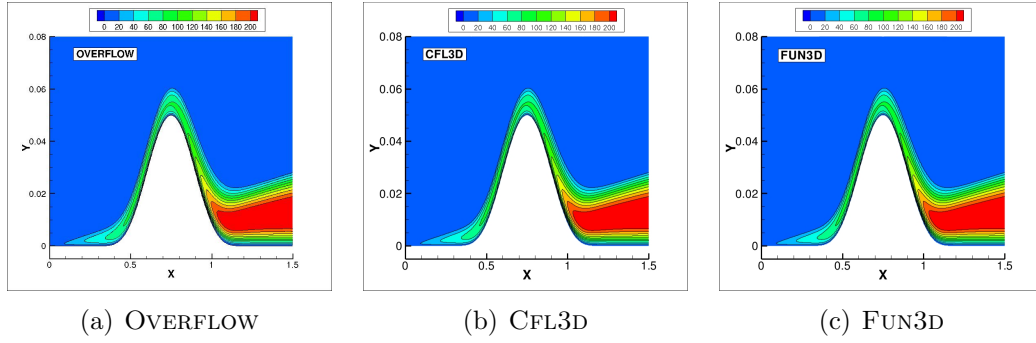
(a) Overflow   (b) Cfl3d   (c) Fun3d

Figure 51: SA eddy viscosity contours, finest grid.

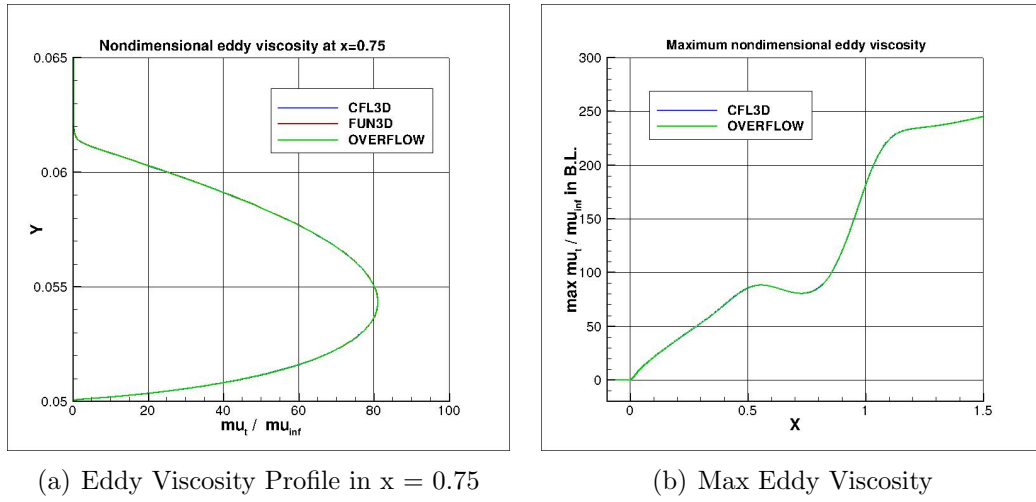(a) Eddy Viscosity Profile in x = 0.75   (b) Max Eddy Viscosity

Figure 52: SA eddy viscosity distributions.
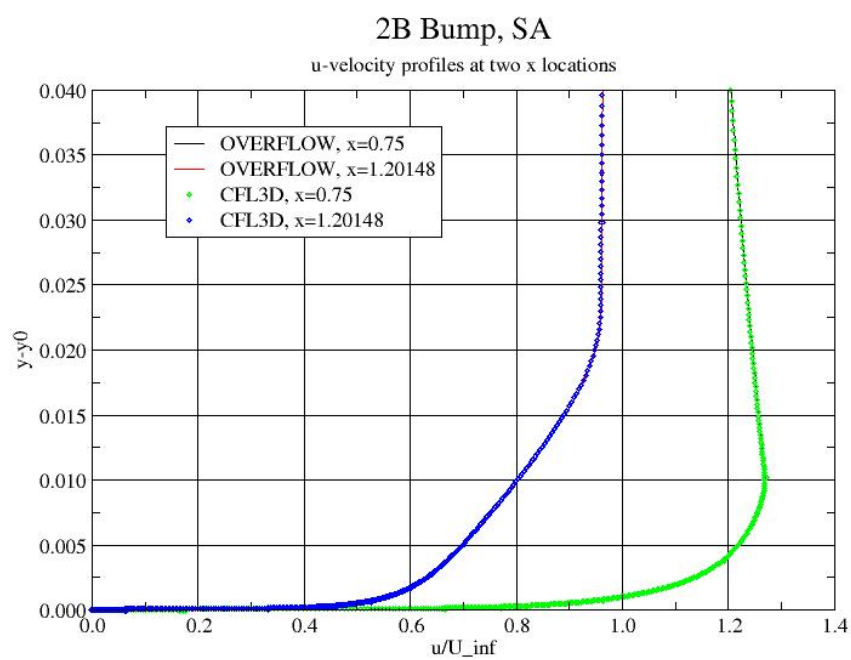
Figure 53: SA scaled u-velocity profiles.

4.2 Overflow SST Results

For the CFL3D and FUN3D tests reported below, the turbulent inflow boundary conditions used for SST were as follows:

$$k_{farfield} = 9 \times 10^{-9} a_\infty^2$$

$$\omega_{farfield} = 1 \times 10^{-6} \frac{\rho_\infty a_\infty^2}{\mu_\infty}$$

where a_∞ is the reference speed of sound.

OVERFLOW assumes that k and ω at the farfield normalized by of u_∞, so that in terms of the OVERFLOW variables $k_{farfield} = \texttt{XKINF} = 2.25 \times 10^{-7}$, $\mu_{farfield} = \texttt{MUTINF} = 0.01$ ($\omega_{farfield}$ is computed internally from these values).

Typical convergence histories are shown in Figure 54, where we strove to get to machine zero whenever possible. As with the SA model, we attribute slow convergence to the discontinuity in the boundary conditions along the bottom boundary.
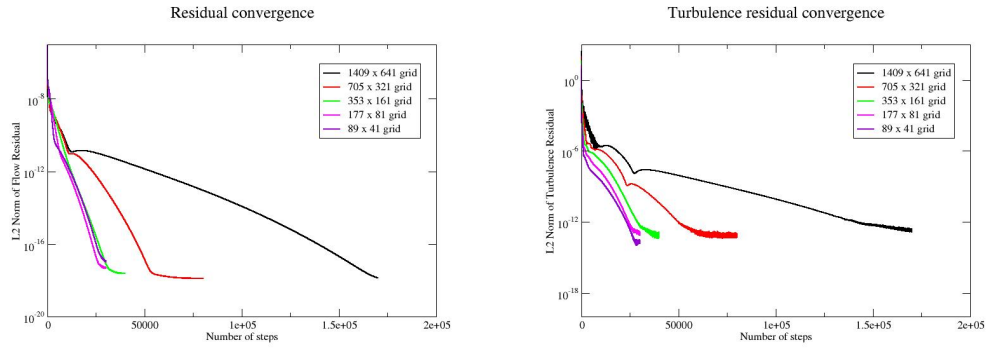

(a) Flow Solver Residual Convergence

(b) Turbulence Model Convergence

Figure 54: SST convergence characteristics, 2D bump.

Figure 55 shows convergence of total drag, pressure drag, viscous drag, and lift for the finest grid for OVERFLOW. All the forces are well converged.
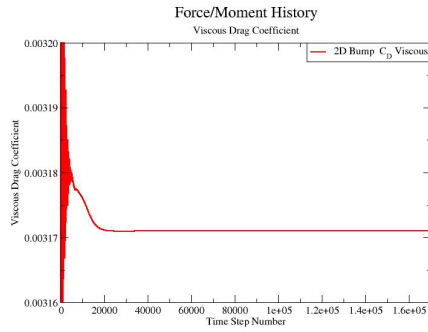
Figure 56 shows the convergence of the wall skin friction coefficient at the bump peak ($x = 0.75$), in front of the peak ($x = 0.6321975$), and aft of the peak ($x = 0.8678025$) with grid size for the three codes. The codes are consistent with one another.
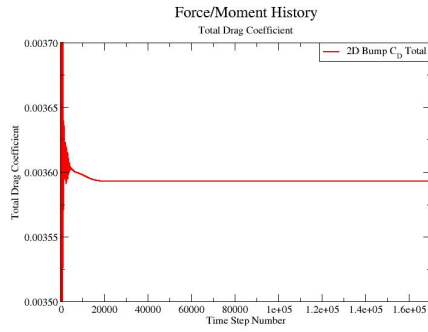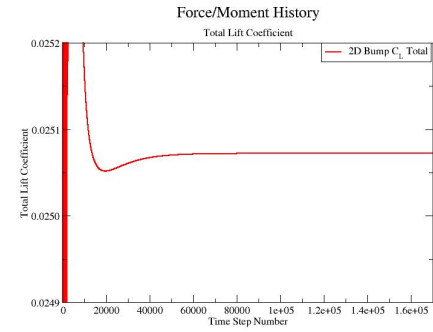
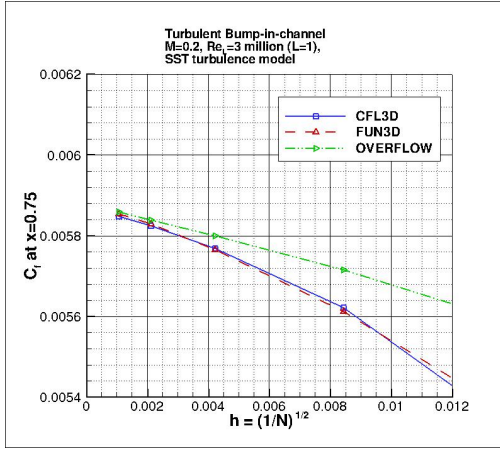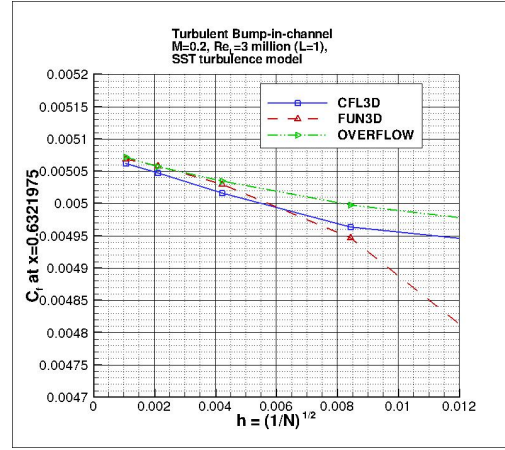(a) Total Drag
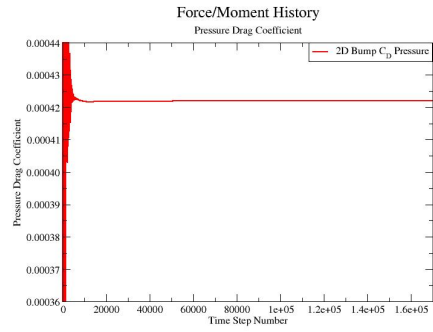
(b) Pressure Drag
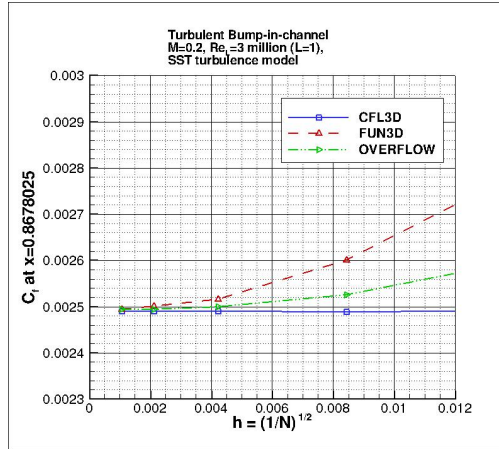
(c) Viscous Drag

(d) Total Lift

Figure 55: SST loads convergence, 2D bump.

(a) C_f at $x = 0.75$

(b) C_f at $x = 0.632197$

(c) C_f at $x = 0.8678025$

Figure 56: SST grid Convergence, 2D bump.

The surface skin friction coefficient from all three codes on the finest 1409×641 grid over the entire bump wall is shown in Figure 57a. The surface pressure coefficient C_p from all three codes on the finest grid, over the entire bump wall, is shown in Figure 57b. The codes are consistent with one another.
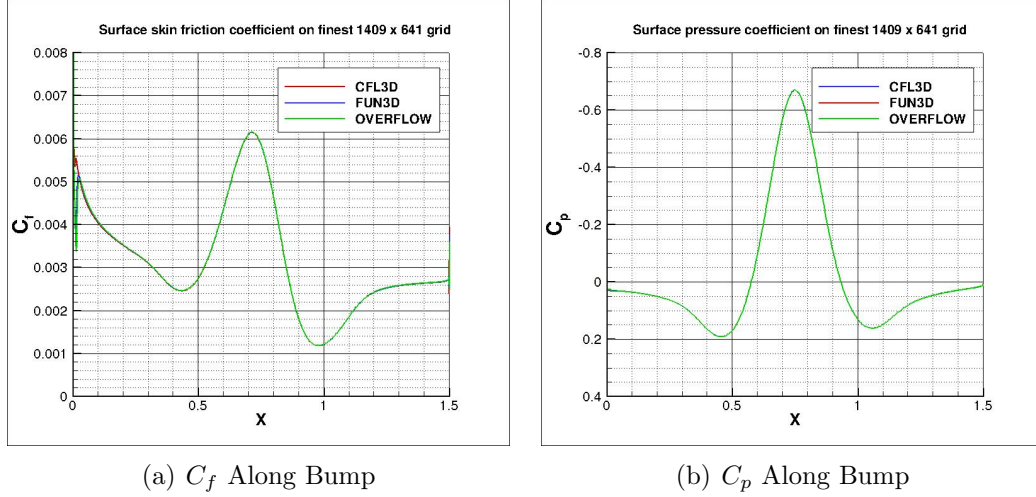

(a) C_f Along Bump

(b) C_p Along Bump

Figure 57: C_f and C_p aong wall: finest grid.

The nondimensionalized eddy viscosity contours, k contours, and ω contours from the three codes on the finest grid are shown in Figure 58 (y-scale expanded for clarity). Results from the three codes on this grid are essentially indistinguishable.

An extracted nondimensional eddy viscosity profile at $x = 0.75$ for the three codes, using the finest grid, is shown in Figure 59. A plot of the maximum nondimensional eddy viscosity as a function of x for OVERFLOW and CFL3D (the TMR website does not provide maximum nondimensional eddy viscosity for FUN3D), is shown in Figure 59b. Agreement among the three codes is excellent.

Nondimensional k and ω profiles at $x = 0.75$ on the finest grid are shown in Figure 60. The three codes are in close agreement.

Scaled u-velocity profiles at two x locations for OVERFLOW and CFL3D are shown in Figure 61. The curves plot atop one another.
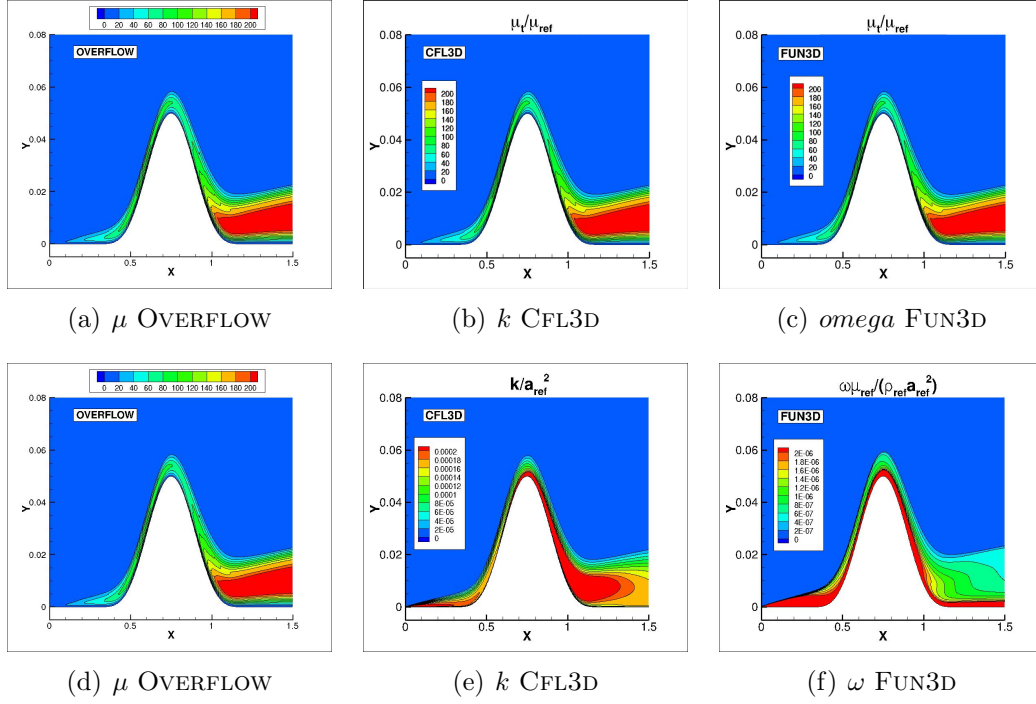
(a) μ OVERFLOW   (b) k CFL3D   (c) *omega* FUN3D

(d) μ OVERFLOW   (e) k CFL3D   (f) ω FUN3D

Figure 58: SST viscous quantity contours, finest grid.

(a) Eddy Viscosity Profile at $x = 0.75$ (b) Maximum Eddy Viscosity
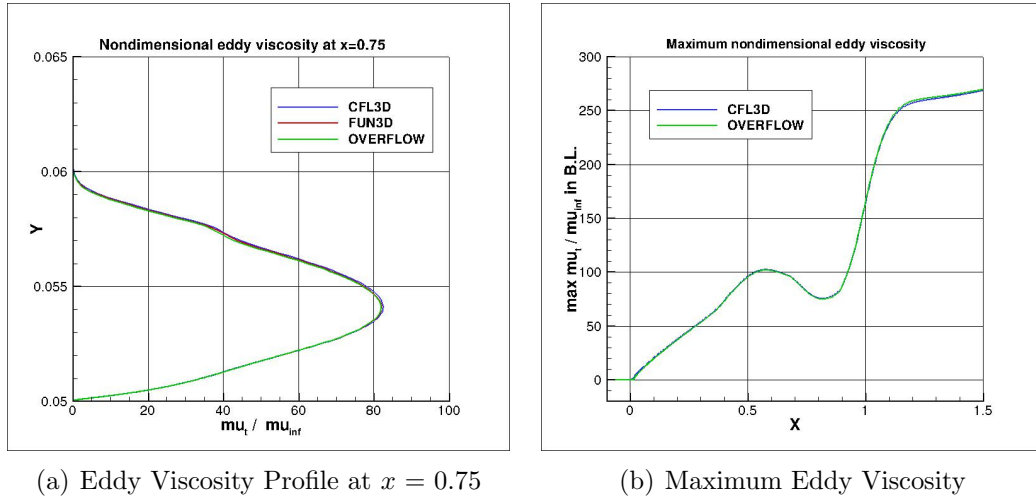
Figure 59: SST eddy viscosity distributions.

58

(a) k profile in y at $x = 0.75$ (b) ω profile in y at $x = 0.75$
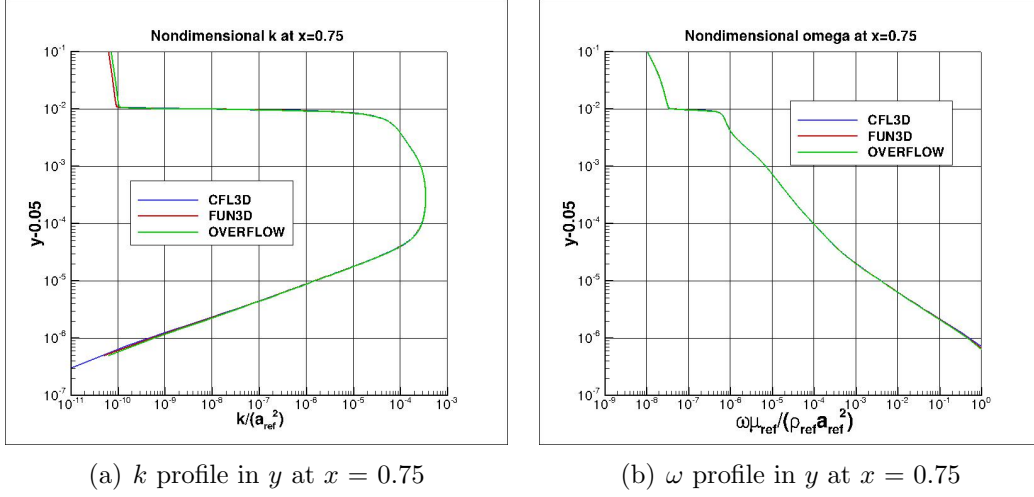
Figure 60: SST k and ω profiles.

4.3 Overflow SST-V Results

Typical convergence histories are shown in Figure 62, where we strove to get to machine zero whenever possible. Again we attribute slow convergence to the discontinuity in boundary conditions.

Figure 63 shows convergence of total drag, pressure drag, viscous drag, and lift for the finest grid using OVERFLOW. All the forces are well converged.

Figure 64 shows the convergence of the wall skin friction coefficient as a function of grid size at the bump peak ($x = 0.75$), in front of the peak ($x = 0.6321975$), and aft of the peak ($x = 0.8678025$) for the three codes. The three codes are consistent with one another as the mesh is refined.

Figure 65 shows: total drag coefficient, pressure drag coefficient, viscous drag coefficient, and total lift coefficient as functions of grid size for the three codes. There are some differences in asymptotic values of pressure drag and viscous drag among the three codes.

The surface skin friction coefficient from the three codes on the finest grid over the entire bump wall is shown in Figure 66a. The surface pressure coefficient C_p from all three codes on the finest grid over the entire bump wall is shown in Figure 66b. The C_p plots lie atop one another, while there are small differences in C_f.

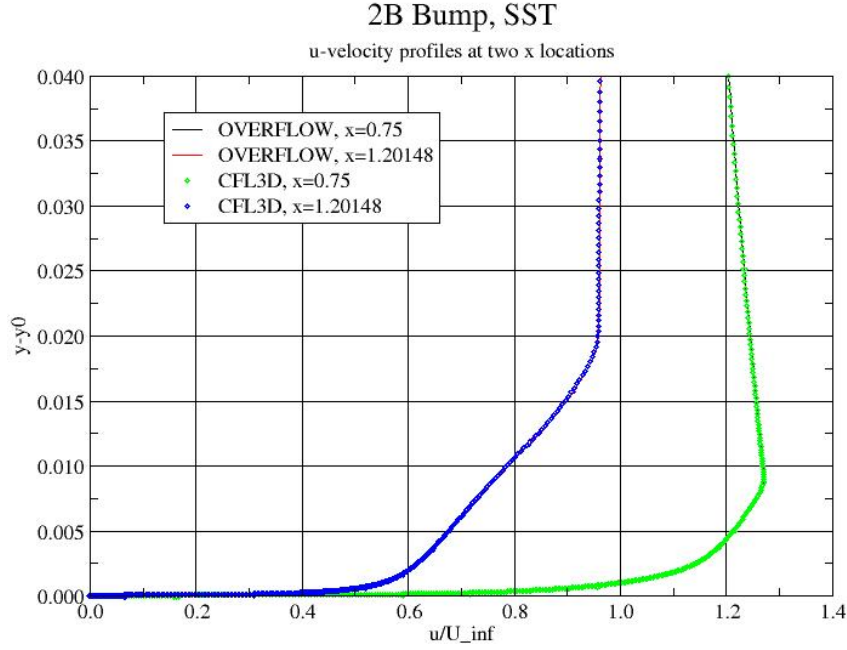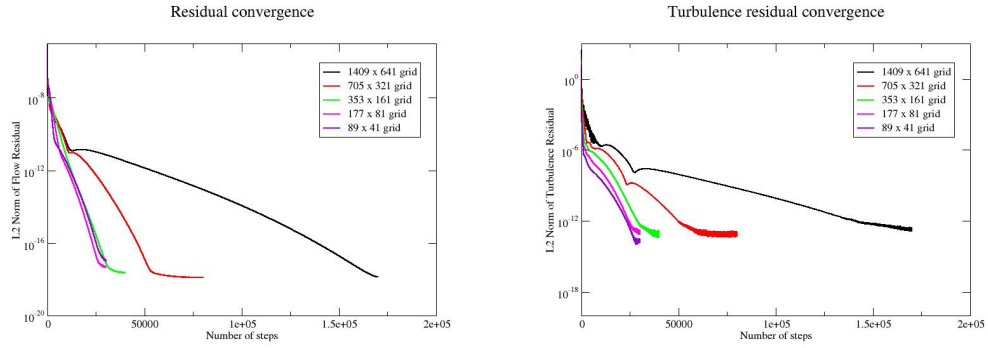The nondimensionalized eddy viscosity contours, k contours, and ω con-

59

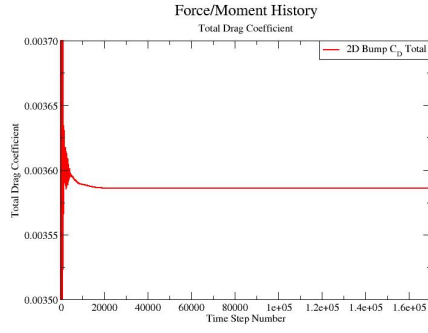Figure 61: SST scaled *u*-velocity profiles.
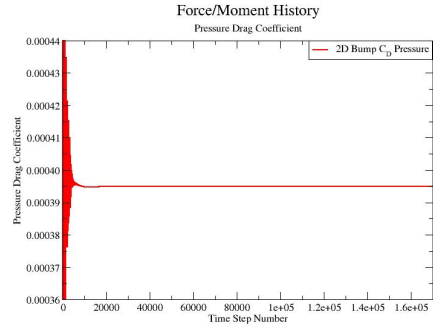

(a) Flow Solver Residual Convergence   (b) Turbulence Model Convergence

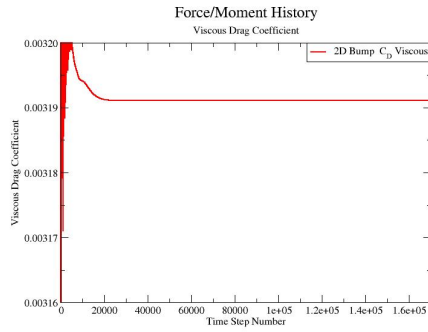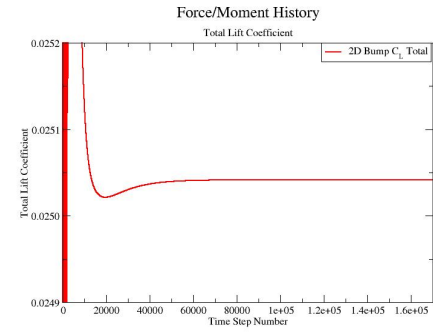Figure 62: SST-V convergence characteristics, 2D bump.

60

(a) Total Drag

(b) Pressure Drag

(c) Viscous Drag

(d) Total Lift

Figure 63: SST-V loads convergence, 2D bump.
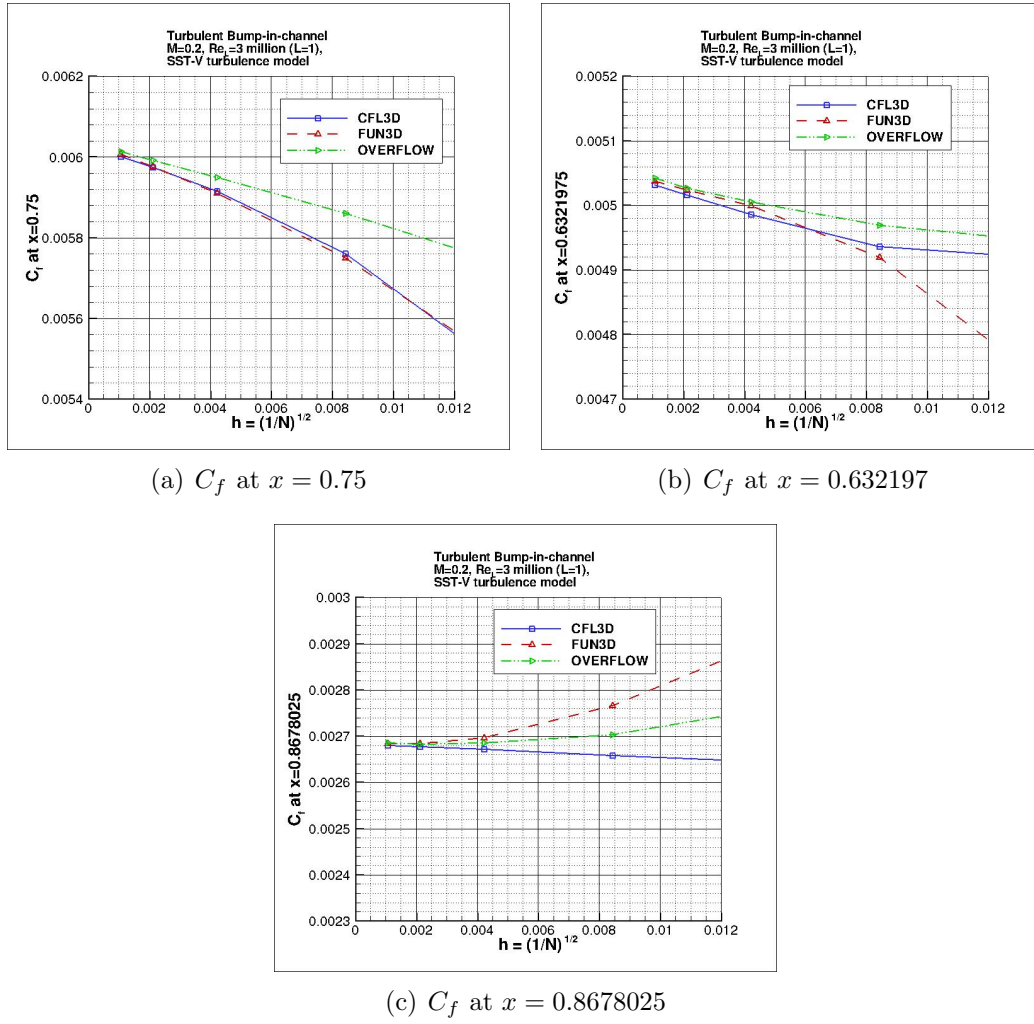
61

(a) C_f at $x = 0.75$

(b) C_f at $x = 0.632197$
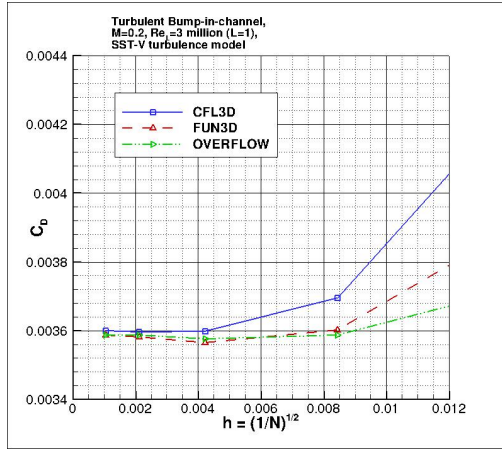

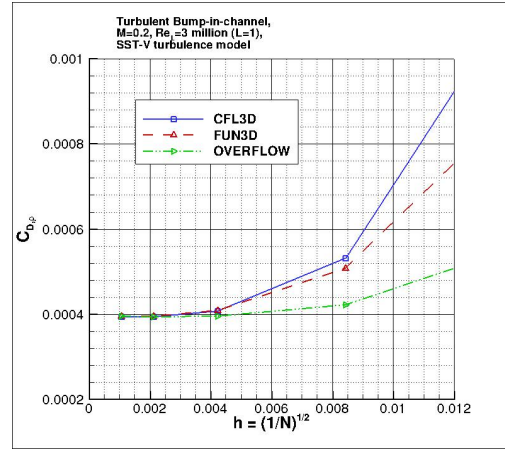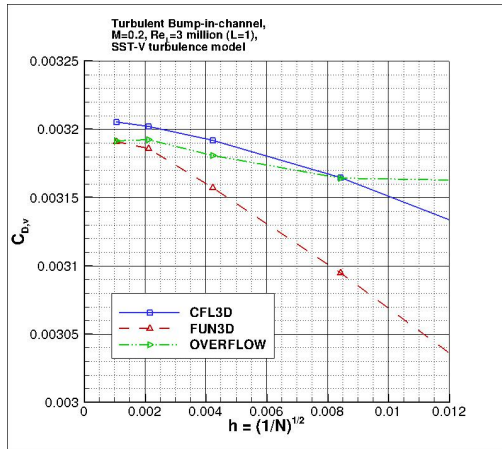(c) C_f at $x = 0.8678025$

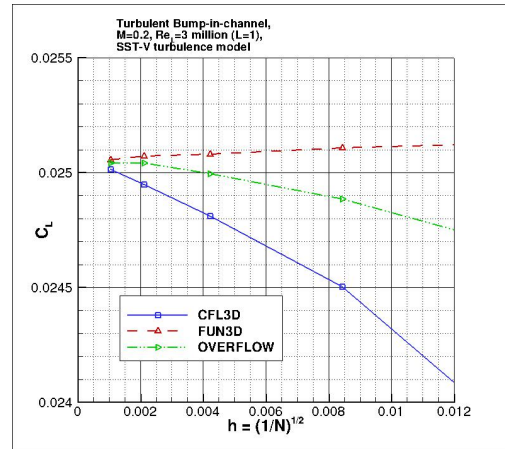Figure 64: SST-V grid convergence, 2D bump.

(a) Total Drag   (b) Pressure Drag

(c) Viscous Drag   (d) Total Lift

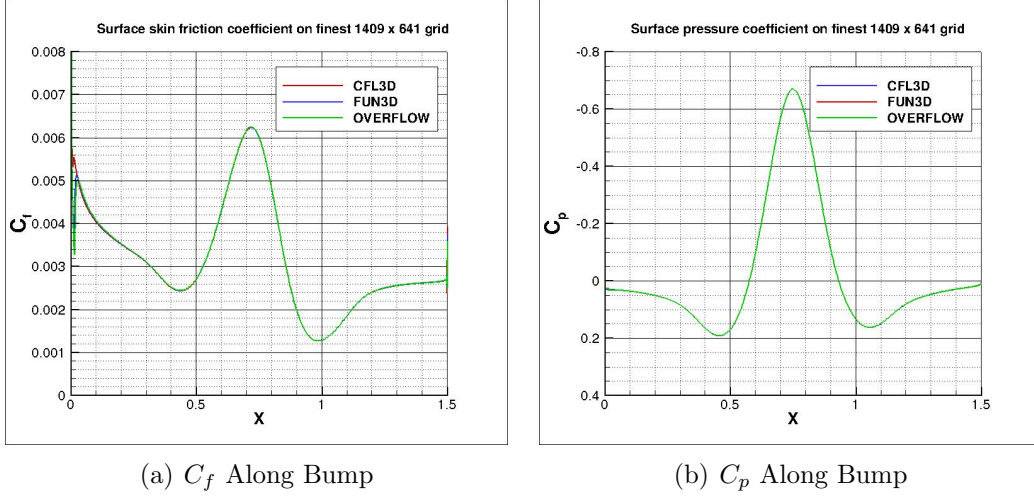Figure 65: SST-V grid convergence, loads.

(a) C_f Along Bump   (b) C_p Along Bump

Figure 66: C_f and C_p along bump, finest grid.

tours from the three codes on the finest grid are shown in Figure 67 (y-scale expanded for clarity). The plots from the three codes on this grid are essentially indistinguishable.

Using the finest grid, an extracted nondimensional eddy viscosity profile at $x = 0.75$ for the three codes is shown in Figure 68a, along with a plot of the maximum nondimensional eddy viscosity as a function of x for OVERFLOW and CFL3D (the TMR website does not provide maximum nondimensional eddy viscosity for FUN3D) in Figure 68b. For the eddy viscosity profile, CFL3D and FUN3D agree with one another, while the OVERFLOW curve is somewhat different. The maximum eddy viscosity plot shows some differences between CFL3D and OVERFLOW.

Nondimensional k and ω profiles at $x = 0.75$ from the finest grid are shown in Figure 69. Both plots show slight differences between OVERFLOW and the other two codes,

Scaled u-velocity profiles at two x locations for OVERFLOW and CFL3D are shown in Figure 70. The curves plot atop one another.
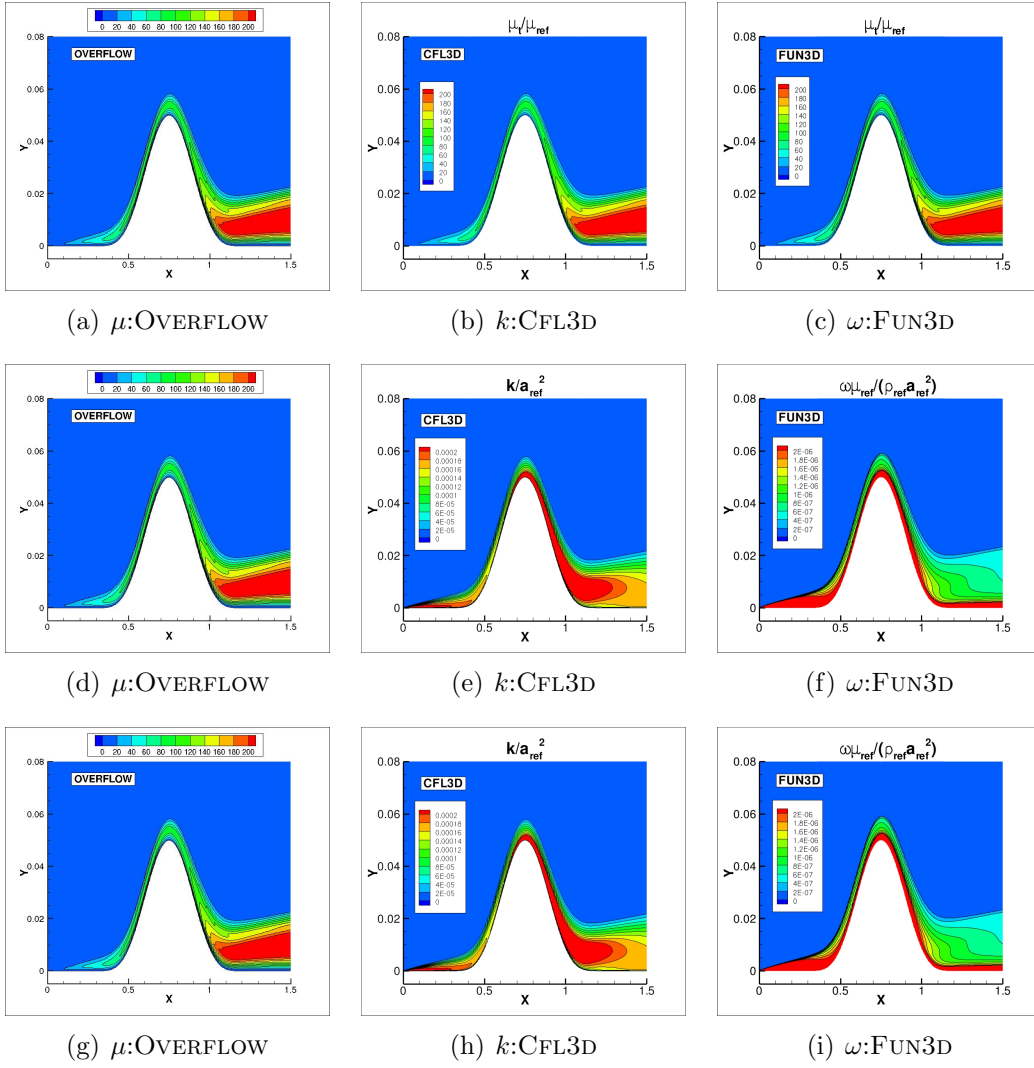
(a) μ:Overflow

(b) k:Cfl3d

(c) ω:Fun3d

(d) μ:Overflow

(e) k:Cfl3d

(f) ω:Fun3d

(g) μ:Overflow

(h) k:Cfl3d

(i) ω:Fun3d

Figure 67: SST-V viscous quantity contours, finest grid.

(a) Eddy Viscosity Profile at $x = 0.75$

(b) Max Eddy Viscosity
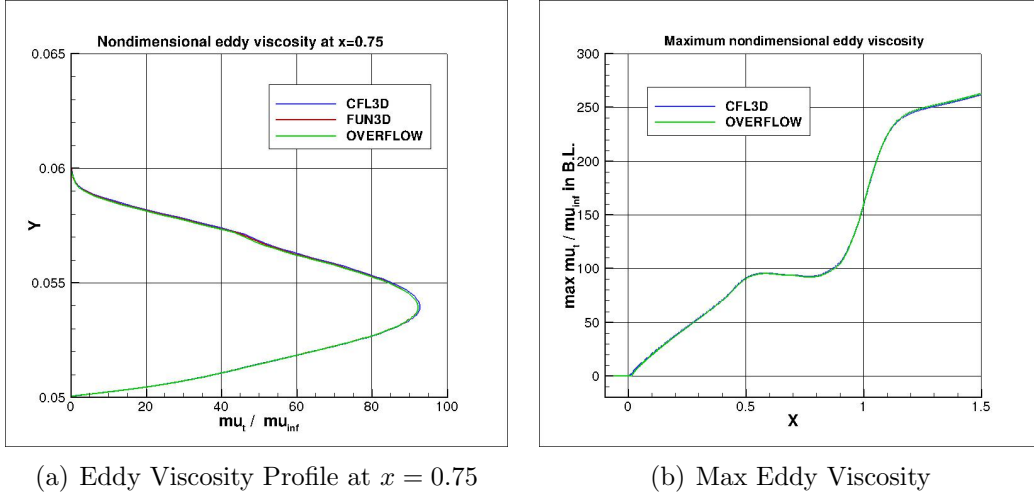
Figure 68: SST-V eddy viscosity distributions.

(a) k profile in y at $x = 0.75$

(b) ω profile in y at $x = 0.75$
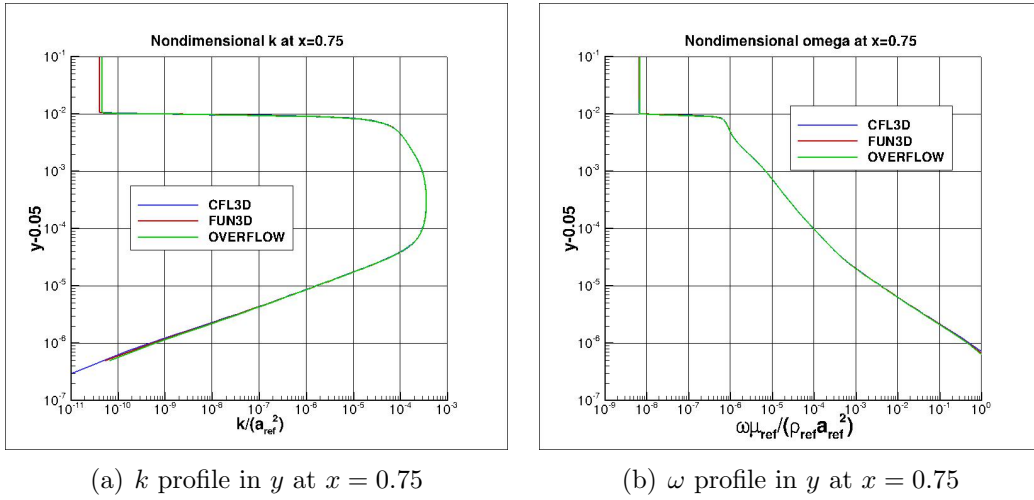
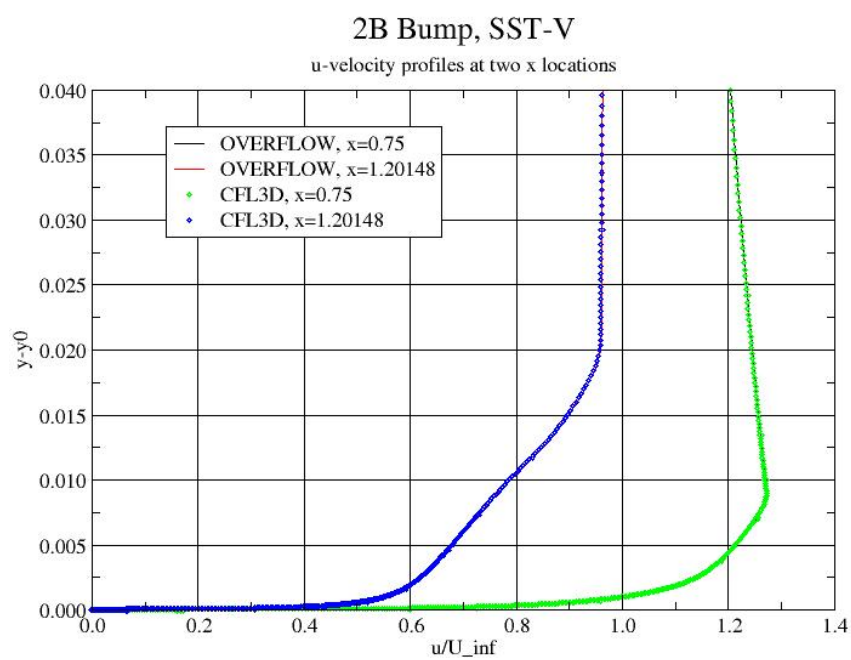Figure 69: SST-V k and ω profiles, finest grid.

66

Figure 70: SST-V scaled *u*-velocity profiles.

5   3D Bump

In this section we present the results of turbulence model verification for OVERFLOW using the TMR 3D Bump-in-channel test case. This case is a three-dimensional version of the 2D Bump-in-channel verification case, with spanwise variation added. In this 3D case the z direction is up and y is the spanwise direction. The case was run at Mach number $M = 0.2$ and Reynolds number $Re = 3$ million, based on a grid length of 1. The body reference area is 1.5 units. The lower wall is a curved, viscous-wall bump extending from $x = 0$ to 1.5 at the two sides of the computational domain $y = 0$ and $y = -1$, but starting and ending further downstream at intermediate y locations. The maximum bump height is 0.05. The definition of the bump at the $y = 0$ plane is: $z = 0.05 * (\sin(\pi x/0.9 - (\pi/3.)))^4$ for $0.3 \leq x \leq 1.2$ along $y = 0$, $z = 0$ for $0 \leq x < 0.3$ and $1.2 < x \leq 1.5$. The x-location of any position on the bump varies in the spanwise direction between $y = 0$ and $y = -1$ according to: $x = x_0 + 0.3(\sin(\pi y))^4$ for $-1 \leq y \leq 0$, where x_0 is any given x-location of the 3D shape at $y = 0$.

The upstream and downstream farfield boundaries extend 25 units from the viscous wall, with symmetry plane boundary conditions imposed on the lower wall between the far field and the solid wall. The upper boundary, at $y = 5.0$, is taken to be a symmetry plane. The left and right walls are also taken to be symmetry planes. Figure 71 shows the layout of this case, along with the boundary conditions.

The grids are taken directly from the TMR website, where details on the formats and other characteristics are available. For this case, the website provides two-dimensional structured grids and a Fortran90 program to translate them into three-dimensional grids. The final dimensions of the three-dimensional grids usable by OVERFLOW are as follows:

- $65 \times 705 \times 321$ (denoted L1)

- $33 \times 353 \times 161$ (denoted L2)

- $17 \times 177 \times 81$ (denoted L3)

- $9 \times 89 \times 41$ (denoted L4)

- $5 \times 45 \times 21$ (denoted L5)

(a) 3D Bump Topology

(b) Bump Layout and Conditions

(c) 3D Bump Shape

Figure 71: 3D bump geometry and boundary conditions.

A portion of the $17 \times 177 \times 81$ grid is shown in Figure 72. The TMR website provides expected Cfl3d and Fun3d results for the SA and SST-V models.
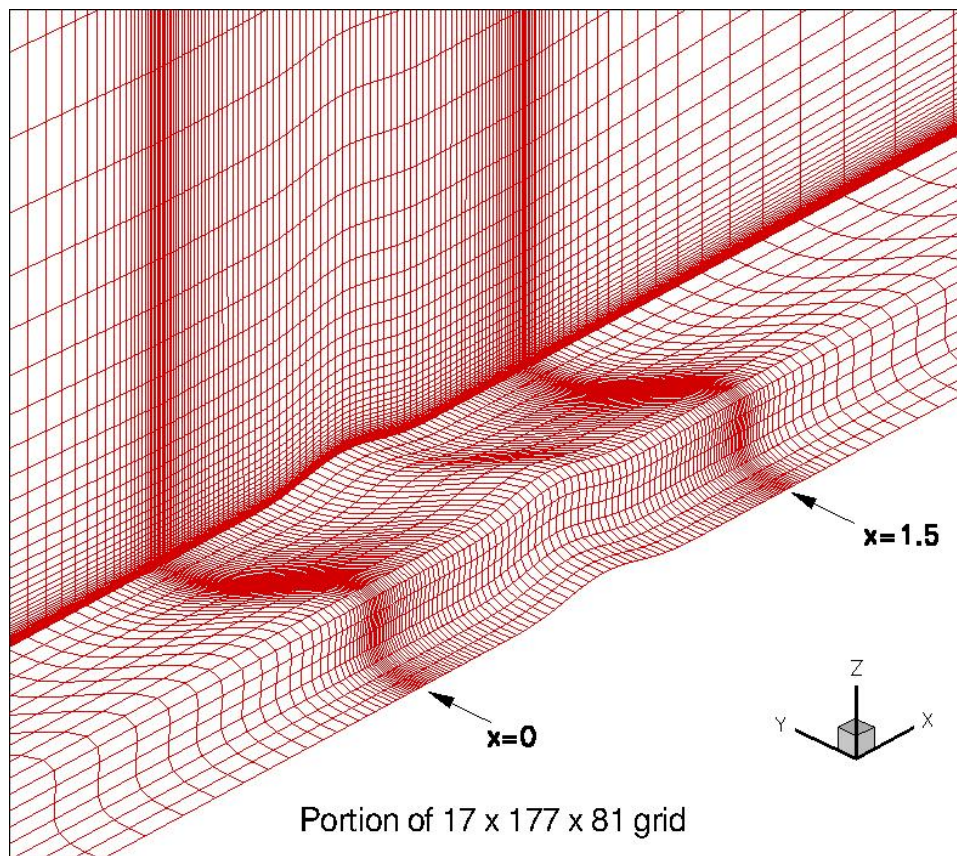

Figure 72: Grid system for 3D bump.

Input files for Overflow were generated with the appropriate boundary and flow conditions. Matrix dissipation with low-Mach preconditioning was used. A sample Overflow input file for the finest grid SA case is shown here:

```
&GLOBAL
    NSTEPS= 95000,  RESTRT= .F.,
    MULTIG= .T.,  FMG   = .T.,  FMGCYC= 100,100,
```

```
    NQT   = 102, NGLVL = 2, WALLDIST = 2,
    /
&FLOINP
    FSMACH= 0.2,  REY   = 3.0E6,  TINF = 540.0,  MUTINF = 0.2,
    /
&VARGAM /

&GRDNAM
    NAME = 'TMR 3D Bump SA',
    /
&NITERS /
&METPRM
    IDISS = 4, BIMIN = -1,
    /
&TIMACU
    DT    = 1.0,  CFLMIN= 5,
    /
&SMOACU
    DIS2 = 0.0, DIS4 = 0.02, FSO = 3,
    /
&VISINP
    CFLT  = 4,
    /
&BCINP
    IBTYP =  41, 33,    5,   17,   17, 17,   17,   17,
    IBDIR =   2, -2,    3,    3,    3, -3,    1,   -1,
    JBCS  =   1,  1,    1,    1,    1,  1,    1,   -1,
    JBCE  =  -1, -1,   -1,   -1,   -1, -1,    1,   -1,
    KBCS  =   1, -1,  193,    1,  514,  1,    1,    1,
    KBCE  =   1, -1,  513,  192,   -1, -1,   -1,   -1,
    LBCS  =   1,  1,    1,    1,    1, -1,    1,    1,
    LBCE  =  -1, -1,    1,    1,    1, -1,   -1,   -1,
    BCPAR1(1) = 1.0, BCPAR2(1) = 1.0, BCPAR1(2) = 1.0,
    /
&SCEINP /
```

5.1 Overflow SA Results

Figure 73 shows OVERFLOW convergence histories for the different grid refinements. Due to the longer run times, we did not require that the residuals be driven all the way to machine zero, although we did produce well-converged loads.
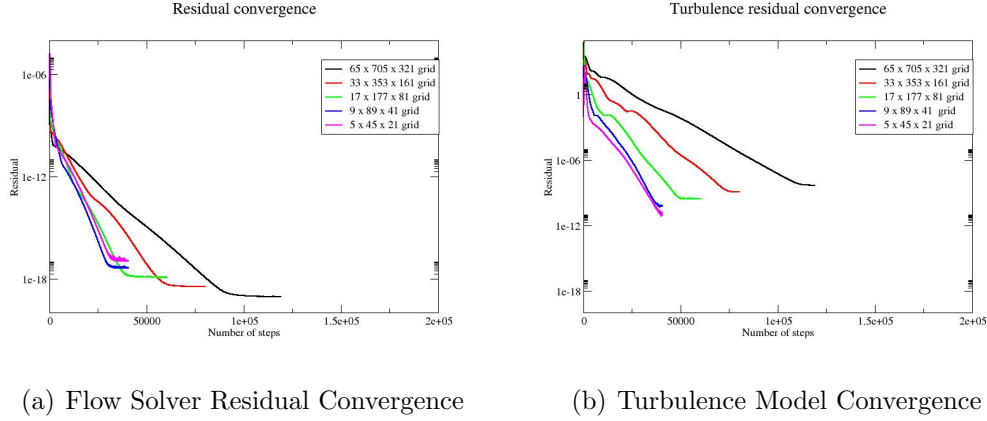

(a) Flow Solver Residual Convergence   (b) Turbulence Model Convergence

Figure 73: SA convergence characteristics, 3D bump.

Figure 74 shows: total drag coefficient, pressure drag coefficient, viscous drag coefficient, and total lift coefficient as functions of iteration number.

Figure 75 shows some forces as functions of a typical mesh length. The codes seem to be producing the same values for loads as the mesh is refined.

In this bump, case the surface skin friction is singular (tends toward infinity) at the leading edge. The finer the grid, the more nearly singular the local behavior on a finite grid. There is also locally anomalous behavior in C_f at the back end of the bump wall (at $x = 1.5$), as is often seen in CFD solutions near trailing edges.

The eddy viscosity contours (nondimensionalized by freestream laminar viscosity) from the three codes on the second-finest $33 \times 353 \times 161$ grid are shown in Figure 76, extracted at $x = 0.3$ (y-scale expanded for clarity). The three plots are very similar to one another.
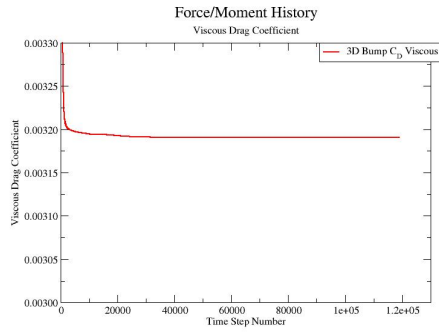
We show eddy viscosity contours for OVERFLOW on the finest grid at $x = 0.3$ in Figure 77. The slight differences between the contour plots on the second-finest and finest grids are due to the difference in grid spacing.
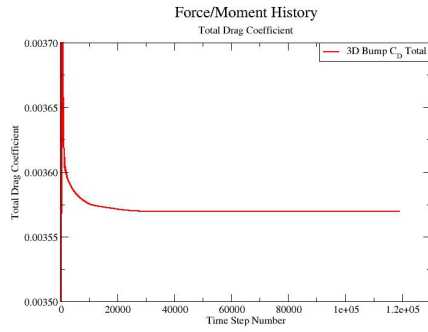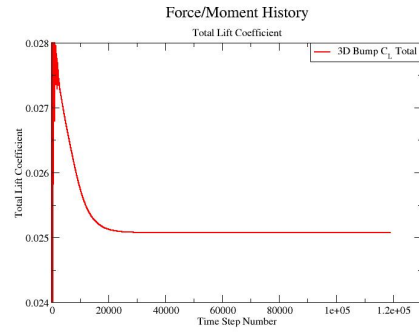
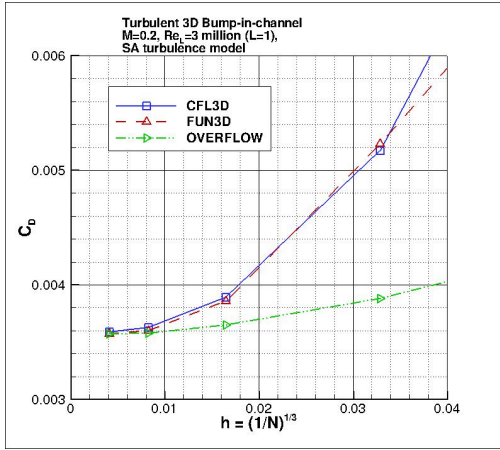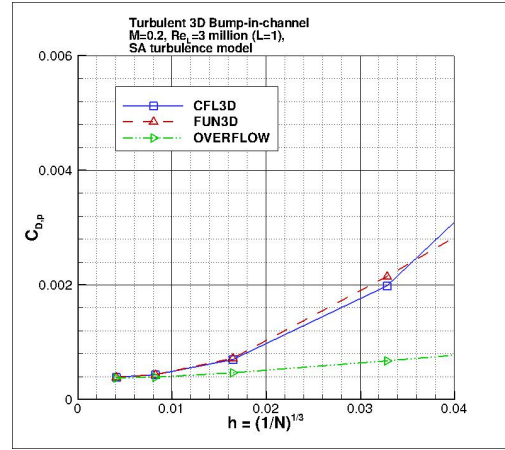(a) Total Drag
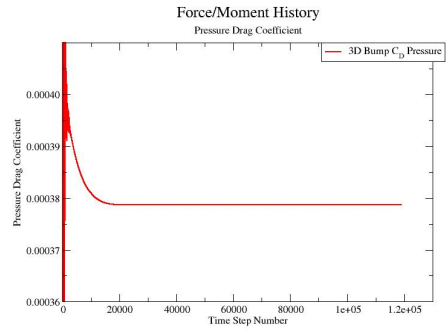
(b) Pressure Drag
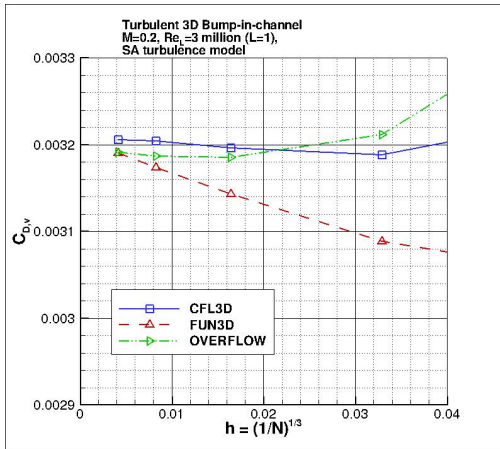
(c) Viscous Drag

(d) Total Lift
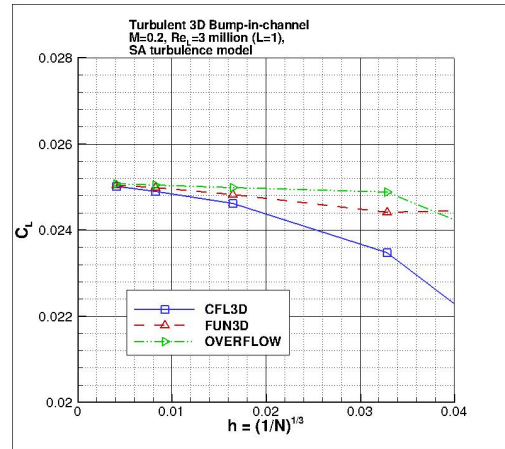
Figure 74: SA loads convergence, 3D bump.

73

(a) Total Drag

(b) Pressure Drag

(c) Viscous Drag

(d) Total Lift

Figure 75: SA grid convergence, 3D bump loads.

74

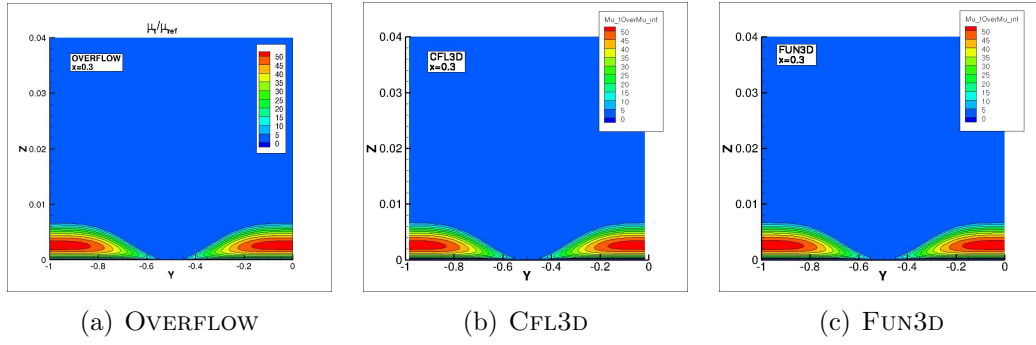(a) OVERFLOW   (b) CFL3D   (c) FUN3D

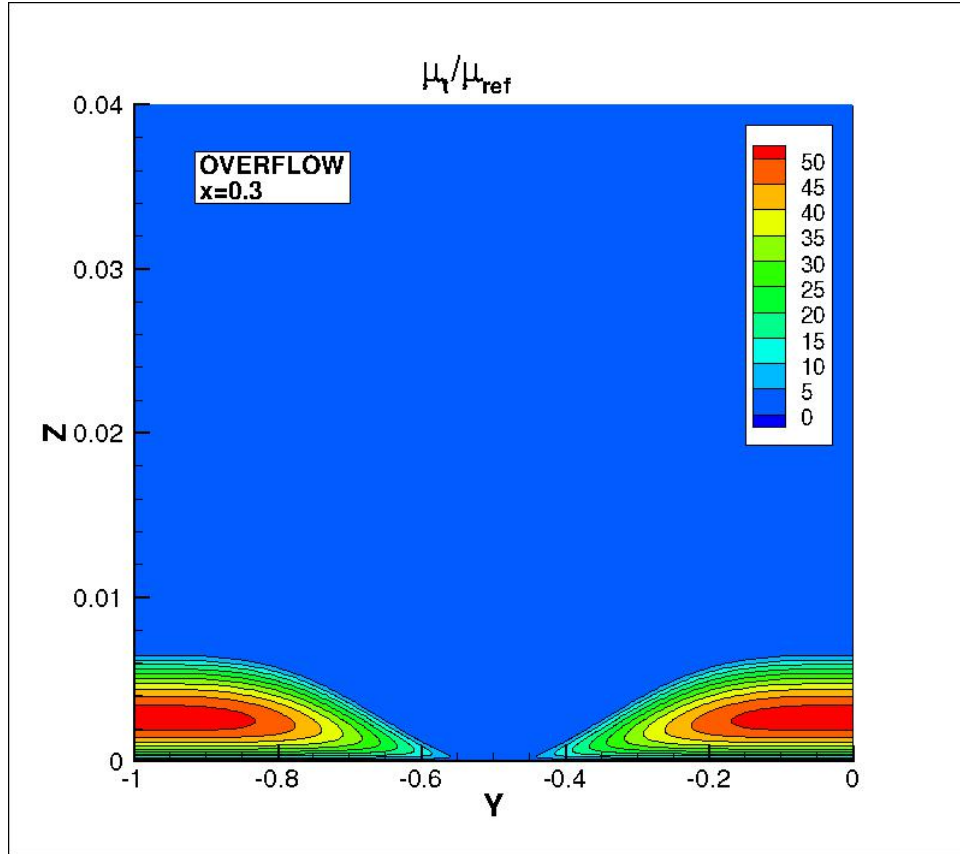Figure 76: SA eddy viscosity contours, 3D bump, second-finest grid.

Figure 77: SA eddy viscosity contours, 3D bump, finest grid.

5.2 Overflow SST-V Results

For the CFL3D and FUN3D tests reported below, the turbulent inflow boundary conditions used for SST-V were as follows:

$$k_{farfield} = 9 \times 10^{-9} a_\infty^2$$

$$\omega_{farfield} = 1 \times 10^{-6} \frac{\rho_\infty a_\infty^2}{\mu_\infty}$$

where a_∞ is the reference speed of sound.

OVERFLOW assumes that k and ω at the farfield are referenced in terms of u_∞, so that in terms of the OVERFLOW variables $k_{farfield} = $ XKINF $= 2.25 \times 10^{-7}, \mu_{farfield} = $ MUTINF $= 0.01$, ($\omega_{farfield}$ is computed internally from those values).

Typical convergence histories are shown in Figure 78, where we drive the residuals to very low values, much lower than are typically needed to ensure well-converged loads.
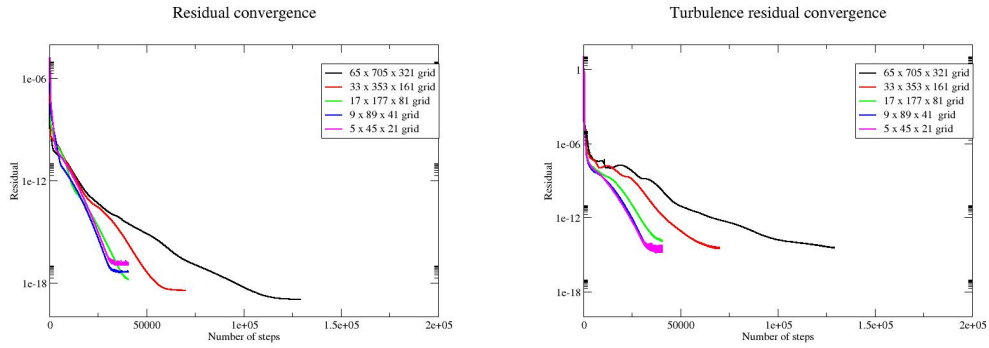
(a) Flow Solver Residual Convergence   (b) Turbulence Model Convergence

Figure 78: SST-V convergence characteristics, 3D bump.

Figure 79 shows some plots of loads versus iteration number on the finest mesh for OVERFLOW. All loads are very well converged and stable.

Figure 80 shows: total drag coefficient, pressure drag coefficient, viscous drag coefficient, and total lift coefficient for the bump as functions of a typical mesh length. The three codes seem to be producing the same asymptotic values as the mesh is refined.
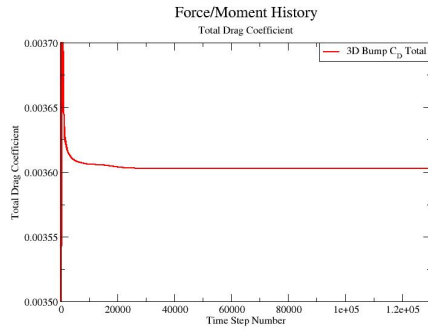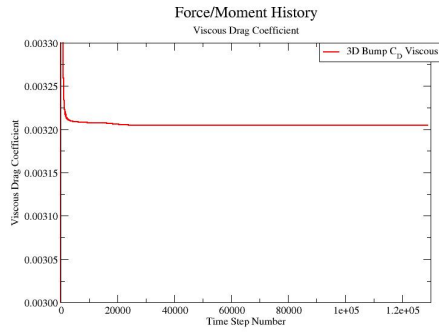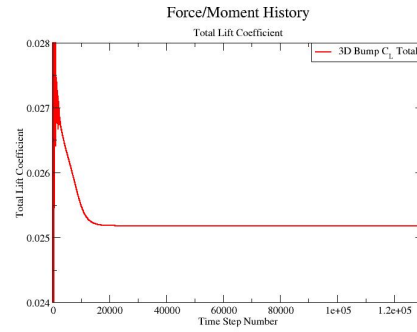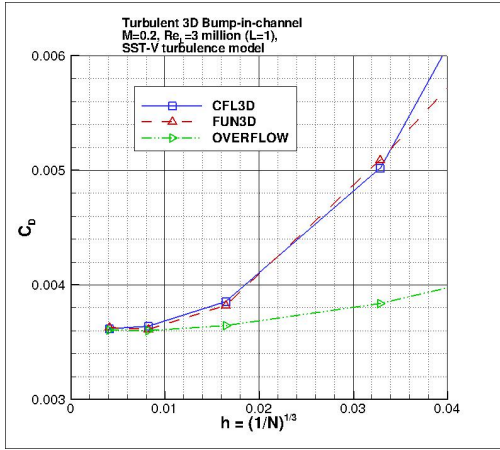
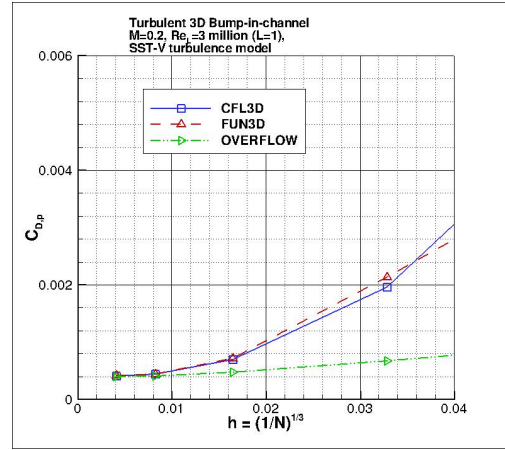(a) Total Drag
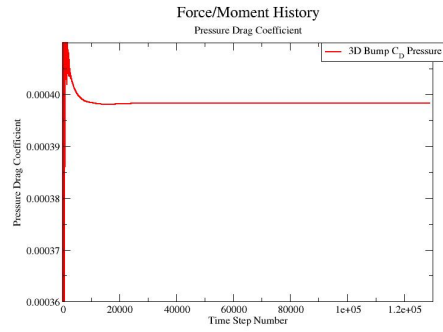
(b) Pressure Drag

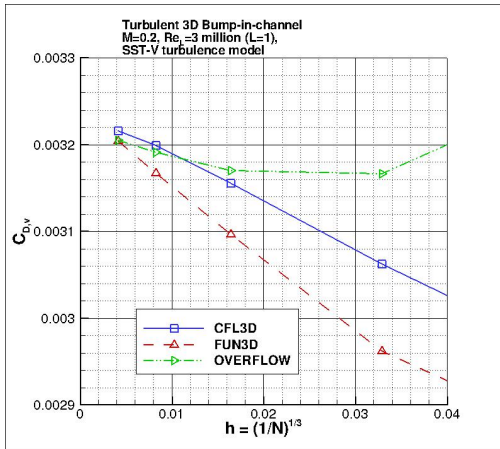(c) Viscous Drag

(d) Total Lift
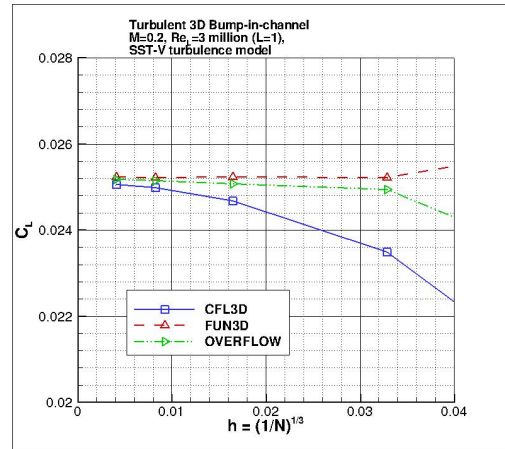
Figure 79: SST-V load histories, 3D bump.

(a) Total Drag

(b) Pressure Drag

(c) Viscous Drag

(d) Total Lift

Figure 80: SST-V grid convergence, loads.

The eddy viscosity contours (nondimensionalized by freestream laminar viscosity), as well as nondimensional k and ω contours from the three codes on the second-finest $33 \times 353 \times 161$ grid, are shown in figures 81, 82, and 83, extracted at two different x-locations (y-scale expanded for clarity). The three codes produce very similar contour plots.

(a) OVERFLOW, $x = 0.3$ (b) CFL3D, $x = 0.3$ (c) FUN3D, $x = 0.3$

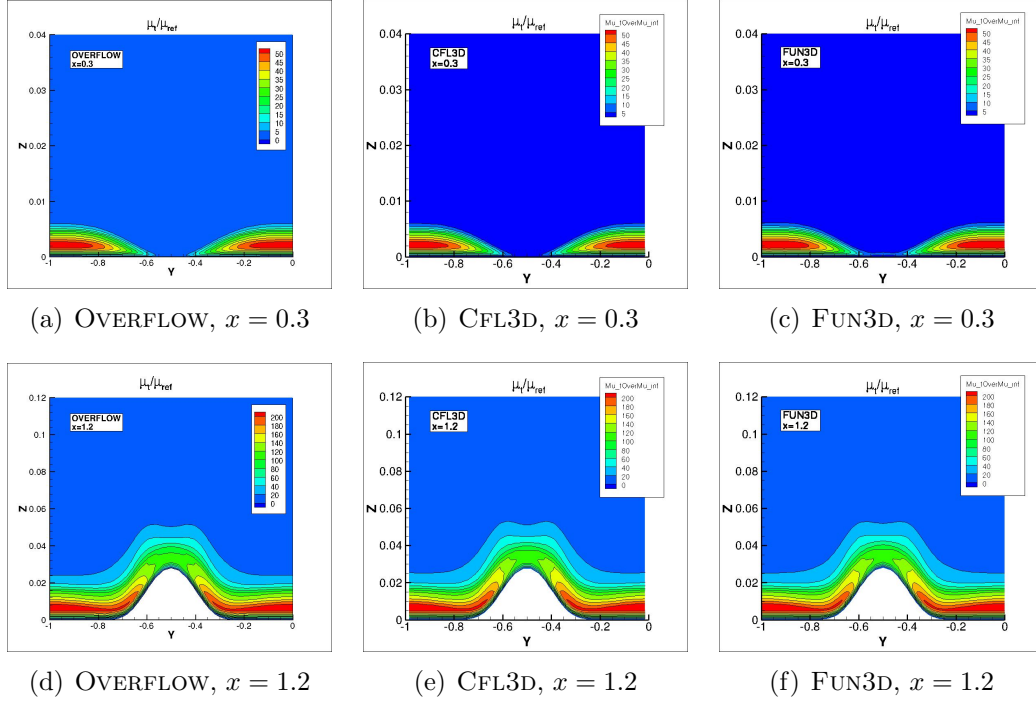(d) OVERFLOW, $x = 1.2$ (e) CFL3D, $x = 1.2$ (f) FUN3D, $x = 1.2$

Figure 81: SST-V eddy viscosity contours, second-finest grid.

Eddy viscosity contour, along with k and ω contours on the finest grid from OVERFLOW are shown in figures 84, 85, and 86. Slight differences occur in the contours plots between the second-finest and finest grids, due to the difference in mesh spacing.
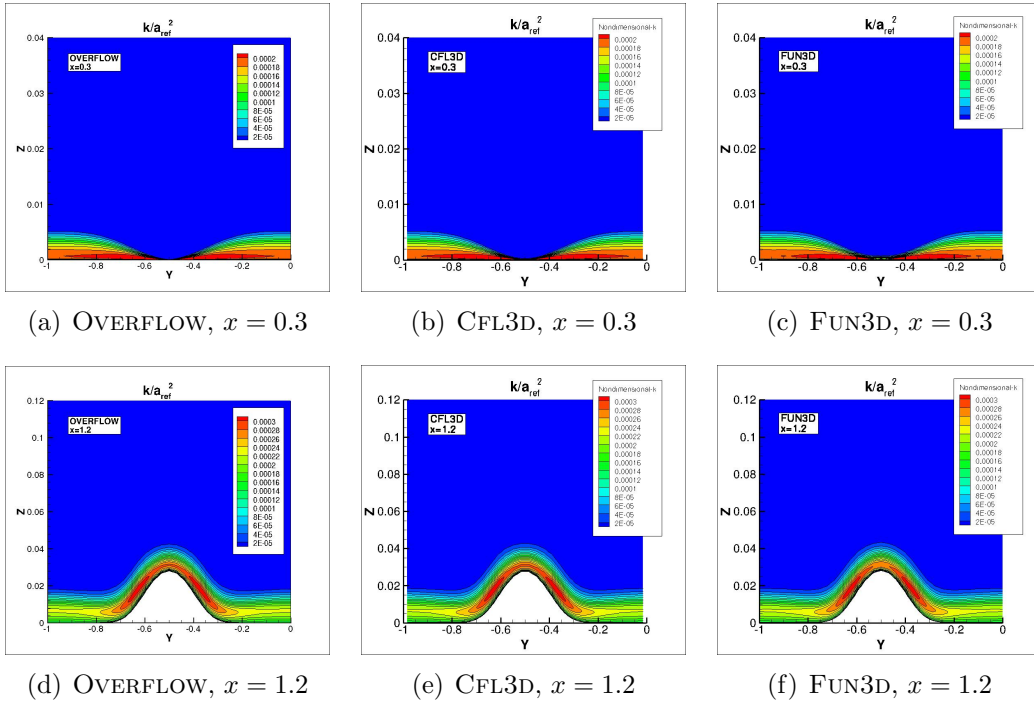
(a) Overflow, $x = 0.3$ (b) Cfl3d, $x = 0.3$ (c) Fun3d, $x = 0.3$

(d) Overflow, $x = 1.2$ (e) Cfl3d, $x = 1.2$ (f) Fun3d, $x = 1.2$

Figure 82: SST-V k contours, second-finest grid.

(a) OVERFLOW, $x = 0.3$ (b) CFL3D, $x = 0.3$ (c) FUN3D, $x = 0.3$

(d) OVERFLOW, $x = 1.2$ (e) CFL3D, $x = 1.2$ (f) FUN3D, $x = 1.2$

Figure 83: SST-V ω contours, second-finest grid.

(a) OVERFLOW, $x = 0.3$ (b) OVERFLOW, $x = 1.2$
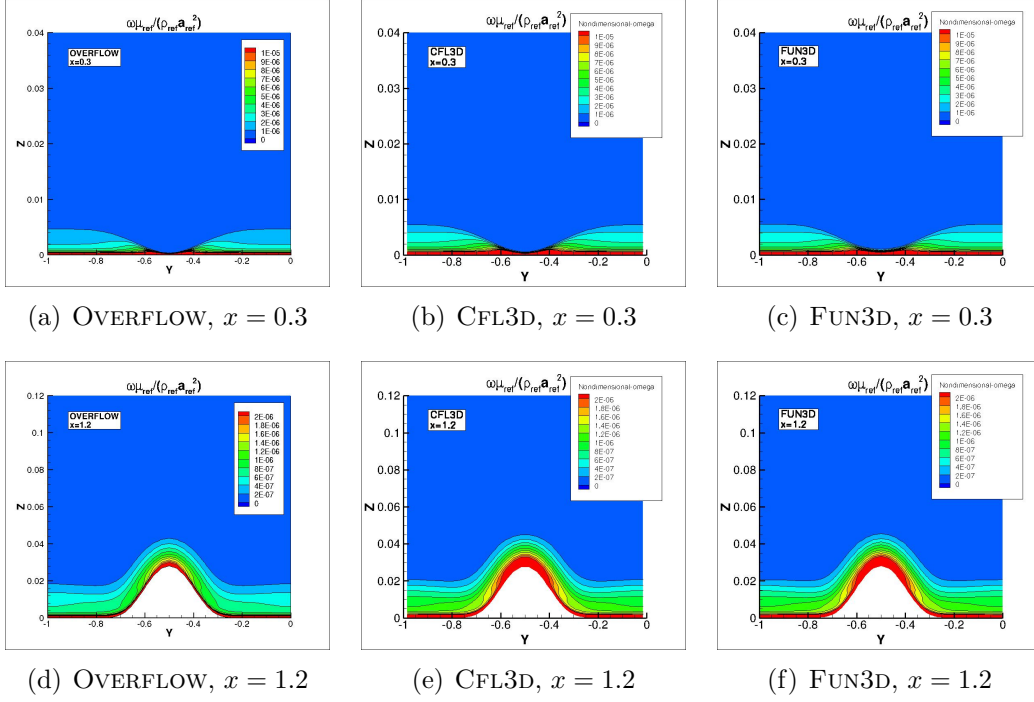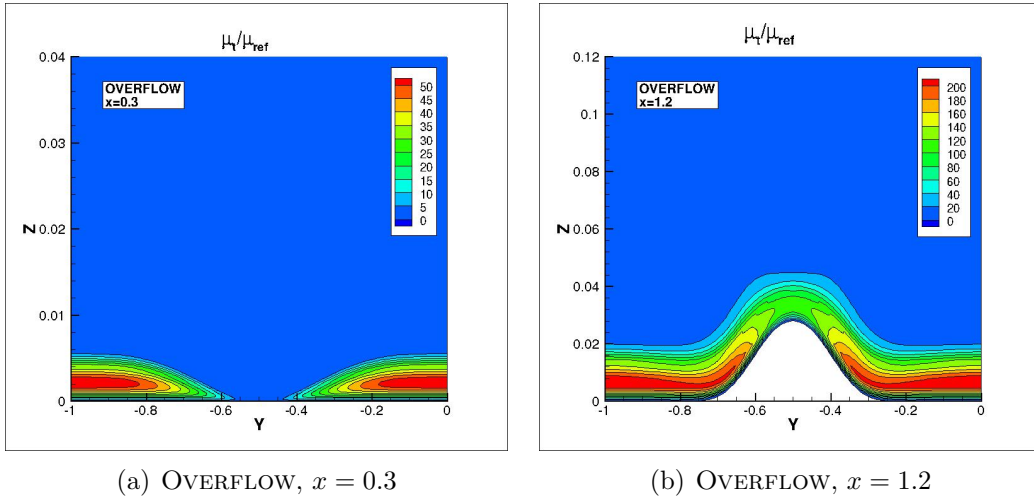
Figure 84: SST-V eddy viscosity contours, finest grid.

(a) OVERFLOW, $x = 0.3$ (b) OVERFLOW, $x = 1.2$
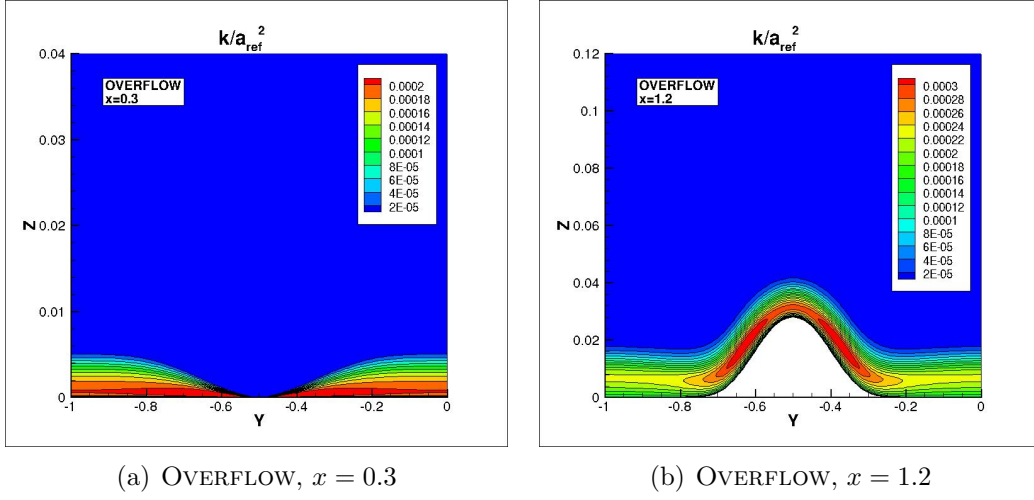
Figure 85: SST-V k contours, finest grid.

(a) OVERFLOW, $x = 0.3$ (b) OVERFLOW, $x = 1.2$
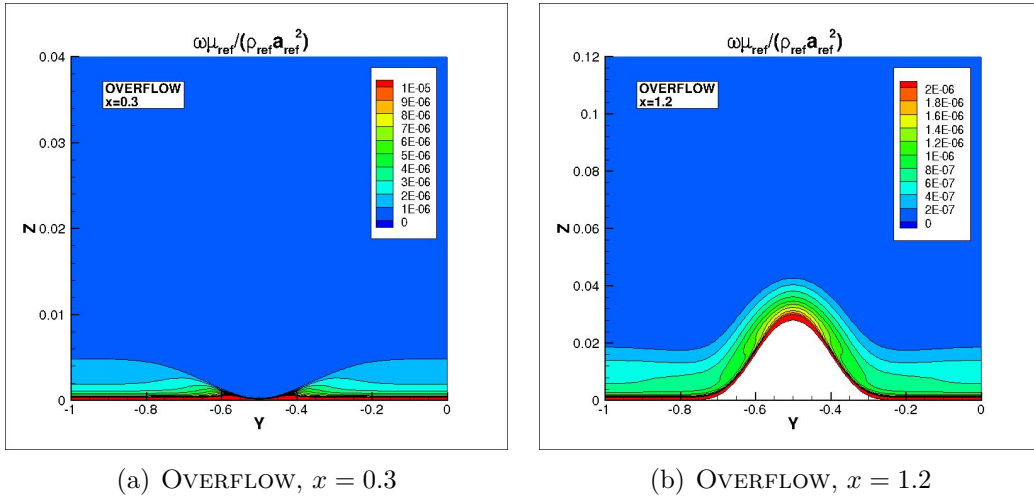
Figure 86: SST-V ω contours, finest grid.

6 Conclusion

We have performed turbulence model verification for the NASA CFD code OVERFLOW on four test cases from the Langley Turbulence Modeling Resource collection. In each case, the results from OVERFLOW compare well with the results from CFL3D and FUN3D. This gives us confidence that the particular turbulence models studied here have been correctly implemented in OVERFLOW. The input files and scripts that produced the OVERFLOW results may, in the near future, be included in the standard set of OVERFLOW test cases.

References

[1] NASA Langley Turbulence Modeling Resource website:
    http://turbmodels/larc.nasa.gov

[2] CFL3D Version 6 website: http://cfl3d.larc.nasa.gov

[3] FUN3D website: http://fun3d.larc.nasa.gov

[4] NASA Langley Turbulence Modeling Resource, 2D Zero
    Pressure Gradient Flate Plate Verification Case:
    http://turbmodels.larc.nasa.gov/flatplate_grids.html

[5] NASA Langley Turbulence Modeling Resource, SA Expected
    Results - 2D Zero Pressure Gradient Flat Plate:
    http://turbmodels.larc.nasa.gov/flatplate_sa.html

[6] NASA Langley Turbulence Modeling Resource, SST/SST-V
    Expected Results - 2D Zero Pressure Gradient Flat Plate:
    http://turbmodels.larc.nasa.gov/flatplate_sst.html

[7] NASA Langley Turbulence Modeling Resource,
    The Spalart-Allmaras Turbulence Model:
    http://turbmodels.larc.nasa.gov/spalart.html

[8] NASA Langley Turbulence Modeling Resource, The
    Menter Shear Stress Transport Turbulence Model:
    http://turbmodels.larc.nasa.gov/sst.html

[9] White, F. M.,**Viscous Fluid Flow**, McGraw-Hill Book Company, New York, 1974, p. 472.

[10] Rajaratnam, N., **Developments in Water Science: Turbulent Jets**, Elsevier Scientific Publishing Company, New York, 1976.

[11] NASA Langley Turbulence Modeling Resource,
    Grids - 2D Planar Shear Verification Case:
    http://turbmodels.larc.nasa.gov/shear_grids.html

[12] NASA Langley Turbulence Modeling Resource,
    Grids - 2D Bump-in-channel Verification Case:
    http://turbmodels.larc.nasa.gov/bump_grids.html